X chromosome and autosomal recombination are differentially sensitive to disruptions in SC maintenance

Katherine Kretovich Billmyre[1]*, Cori K. Cahoon[1,2]*, G. Matthew Heenan[1], Emily Wesley[1,5], Zulin Yu[1], Jay R. Unruh[1], Satomi Takeo[3], and R. Scott Hawley[1,4]

[1] Stowers Institute for Medical Research, Kansas City, MO, 64110, United States of America
[2]Institute of Molecular Biology, Department of Biology, University of Oregon, Eugene, United States of America
[3] Department of Biological Sciences, Tokyo Metropolitan University, Japan
[4] Department of Molecular and Integrative Physiology, University of Kansas Medical Center, Kansas City, KS, 66160, United States of America
[5] University of Missouri-Kansas City, Kansas City, MO, 64110, United States of America
* These authors contributed equally

Corresponding Author:
R. Scott Hawley
Stowers Institute for Medical Research
Kansas City, MO 64110
Phone (816) 926-4427
Fax (816) 926-2060
rsh@stowers.org

Key words: synaptonemal complex, meiosis, homologous recombination, crossing over

Abstract (150 words)

The synaptonemal complex (SC) is a conserved meiotic structure that regulates the repair of double strand breaks (DSBs) into crossovers or gene conversions. The removal of any central region SC component, such as the *Drosophila melanogaster* transverse filament protein C(3)G, causes a complete loss of SC structure and crossovers. To better understand the role of the SC in meiosis, we used CRISPR/Cas9 to construct three in-frame deletions within the predicted coiled-coil region of the C(3)G protein. These three deletion mutants disrupt SC maintenance at different times during pachytene and exhibit distinct defects in key meiotic processes, allowing us to define the stages of pachytene when the SC is necessary for homolog pairing and recombination. Our studies demonstrate that the *X* chromosome and the autosomes display substantially different defects in pairing and recombination when SC structure is disrupted, suggesting that the *X* chromosome is potentially regulated differently than the autosomes.

Introduction

Several facets of meiosis ensure the faithful inheritance of chromosomes from parents to offspring. During the creation of eggs and sperm the genome must be reduced to a haploid state containing a single set of chromosomes; the failure to properly segregate chromosomes results in chromosome missegregation, leading to gametes with an incorrect number of chromosomes. Indeed, errors in meiotic chromosome segregation are the leading cause of miscarriage and aneuploidy in humans, which can result in chromosomal disorders such as Down syndrome and Turner syndrome (reviewed in (Hassold et al., 2007)).

59 Proper segregation of chromosomes during meiosis relies on the formation of
60 programmed double-strand breaks (DSBs), which are initiated when the evolutionarily
61 conserved type II DNA topoisomerase-like protein, Spo11 (Mei-W68 in *Drosophila*),
62 forms programmed DSBs (Keeney et al., 1997; McKim and Hayashi-Hagihara, 1998).
63 These DSBs are then repaired as crossover or gene conversion events (Fig 1A,B).
64 Crossovers mature into chiasmata, which physically hold homologous chromosomes
65 together from nuclear envelope breakdown until homolog separation at anaphase I, thus
66 ensuring proper segregation of chromosomes (Nicklas, 1974). The placement of
67 crossover events is highly non-random and is strictly regulated by multiple processes
68 (Hughes et al., 2018). First, crossover interference prevents two crossovers from
69 occurring in close proximity to each other (Berchowitz and Copenhaver, 2010). Second,
70 crossovers are excluded from the heterochromatin. Third, as a result of the centromere
71 effect, crossing over is also reduced in those euchromatic regions that lie in proximity to
72 the centromeres (Hughes et al., 2018). Finally, even within the medial and distal
73 euchromatin, crossing over is substantially higher toward the middle of the chromosome
74 arms (Szauter, 1984). These constraints do not affect the frequency or distribution of gene
75 conversion events, which appear to be randomly distributed throughout the euchromatin
76 (Crown et al., 2018; Miller et al., 2016, 2012). Thus, the control of crossover distribution may
77 act at the level of DSB fate choice, rather than in determining the position of DSBs.
78 Previous studies have suggested that the synaptonemal complex (SC), a large protein
79 structure that forms between homologous chromosomes, may play a role in controlling
80 crossover distribution (Libuda et al., 2013). The SC is a highly conserved tripartite structure,
81 with two lateral elements and a central region (Fig 1C) (reviewed in (Cahoon and

82 Hawley, 2016; Zickler and Kleckner, 2015, 1999)). The central region is composed of
83 transverse filament and central element proteins, while the lateral element proteins
84 connect the central region to the chromosome axes (Fig 1C). The known proteins that
85 make up the *Drosophila* central region include the main transverse filament protein
86 C(3)G, the transverse filament-like protein Corolla, and the central element protein
87 Corona (CONA) (Collins et al., 2014; Page et al., 2008; Page and Hawley, 2001).
88 Work in *C. elegans* has shown that the SC functions to monitor crossover
89 placement by preventing additional crossover designation in a region adjacent to an
90 existing crossover precursor (Libuda et al., 2013; Nadarajan et al., 2017). Furthermore,
91 there is evidence in *S. cerevisiae* that Zip1, a transverse filament protein, has two
92 separable functions - one in building the SC and the other in recombination (Storlazzi et
93 al., 1996; Voelkel-Meiman et al., 2016). Based on what is known in other model
94 systems, it is likely that the *Drosophila* SC is also playing a role in regulating the fate of
95 DSBs and monitoring crossover placement.
96 In *Drosophila*, approximately 24 DSBs are formed in early pachytene. This
97 occurs in the context of fully formed SC after chromosome synapsis is already complete
98 (Lake et al., 2013; Lindsley et al., 1977; Mehrotra and McKim, 2006). In the absence of
99 the central region of the SC, DSB formation is substantially reduced, but not eliminated.
100 Nonetheless, even in the presence of residual DSBs, there is a complete loss of
101 crossover formation (Collins et al., 2014; Hughes et al., 2018; Mehrotra and McKim,
102 2006; Page et al., 2007). The abolishment of the central region of the SC also results in
103 a high frequency of unpaired homologs during pachytene (Christophorou et al., 2013;
104 Joyce et al., 2013; Sherizen et al., 2005; Takeo et al., 2011). In addition to disrupting

105 meiotic pairing, the loss of any of the known central region components in the (pre-
106 meiotic) mitotic region of the ovaries also impairs mitotic pairing of the *2nd* and *3rd*
107 chromosomes (Christophorou et al., 2013).

108 Since the vast majority of SC mutants are null mutants and therefore fail to form
109 any SC structure, it is difficult to investigate the interactions of the wildtype versions of
110 these proteins at the protein level or discover how the SC is involved in DSB repair and
111 fate choice. In *Drosophila*, the study of transgenes carrying in-frame deletions of either
112 the N- or C-terminal globular domains of C(3)G have shown that both of these regions
113 are required for proper SC assembly and crossover formation (Jeffress et al., 2007).
114 However, these defects were too severe to allow us to investigate the function of the SC
115 in crossover placement and formation. One domain which has not been tested is the
116 large predicted coiled-coil domain in C(3)G. Coiled-coil domains are a key conserved
117 feature of transverse filament proteins across many organisms and are known to be
118 important for protein-protein interactions (Lupas and Bassler, 2017).

119 Here we characterize three in-frame deletion mutations in the coiled coil domain
120 of the *Drosophila melanogaster c(3)G*, all of which cause a partial loss of SC function at
121 different stages in early meiosis. We take advantage of the different stages of SC loss
122 to examine when the SC is necessary for multiple meiotic events such as pairing and
123 recombination. Unlike any previously characterized *Drosophila* meiotic mutants (Baker and
124 Hall, 1976; Hughes et al., 2018; Parry and Sandler, 1974), the effects of these mutants on *X*
125 chromosome recombination is different from their effects on autosomal recombination. We
126 infer from this observation that chromosomes can respond differently to a failure in SC
127 maintenance. We also show that the SC in early pachytene is important for the

128 maintenance of euchromatic pairing, especially in the centromere-distal regions of the
129 chromosome arms. The maintenance of *X* chromosome pairing is more sensitive to SC
130 defects than is pairing maintenance on the autosomes, suggesting there may be
131 additional chromosome-specific processes that mediate pairing. These mutants allow us
132 for the first time to examine the temporal requirement for the synaptonemal complex in
133 crossover placement and maintenance of pairing.
134

135 ## Results

136 **A 213 amino acid in-frame deletion within the coiled-coil region of C(3)G impairs**
137 **the maintenance of the SC in early-mid pachytene**

138 The two previous studies of the functional anatomy of C(3)G have relied on the analysis
139 of transgenic constructs bearing in-frame deletions (Jeffress et al., 2007; Page and
140 Hawley, 2001). While extremely useful, transgenes have the disadvantage of non-
141 endogenous expression levels and improper temporal expression. Based on previous
142 studies in *S. cerevisiae* (Tung and Roeder, 1998) and in *Drosophila* (Page and Hawley,
143 2001), CRISPR/Cas9 was employed to construct an in-frame deletion, $c(3)G^{cc\Delta 1}$,
144 removing the base pairs encoding 213 amino acids (L340-A552) from the 488 amino
145 acid predicted coil-coiled domain of C(3)G (Fig 2A, See Methods).

146 We first asked if $c(3)G^{cc\Delta 1}$ mutants retained the ability to assemble and
147 disassemble the SC with normal kinetics. In wild type flies, components of the central
148 region of the SC are associated with paired centromeres during the pre-meiotic mitotic
149 divisions (Christophorou et al., 2013; Joyce et al., 2013). By early pachytene these
150 proteins are assembled as tripartite SC that is visible as long, continuous tracks of

151 Corolla and C(3)G (Fig 2B, Fig 2.1A). The SC remains fully assembled until mid-late
152 pachytene (stages 5/7), at which point the SC is removed from the euchromatic
153 chromosome arms but remains at the centromeres in mid pachytene (Fig 1B) (reviewed
154 (Hughes et al., 2018)). We assessed SC assembly in homozygous *c(3)G*$^{cc\Delta 1}$ females
155 using a Corolla antibody to mark the central region of the SC. In early pachytene the
156 total length of the SC was similar to wildtype with a decrease in total SC length
157 occurring in early-mid pachytene and a significant decrease in mid pachytene (Fig 2B,C;
158 p=0.01). However, the SC which formed in early-mid pachytene showed obvious
159 discontinuities (Fig 2B).

160 To determine whether or not the removal of a large region of the coiled-coil
161 domain in *c(3)G*$^{cc\Delta 1}$ mutants changed the tripartite structure of the SC, we measured the
162 distance between the C-termini of C(3)G. This was accomplished using a
163 superresolution technique, Stimulated Emission Depletion (STED), in conjunction with a
164 C(3)G C-terminal specific antibody (Anderson et al., 2005; Collins et al., 2014). In wild
165 type controls the distance between the C-termini of C(3)G was 118.4 nm (±0.6 nm
166 SEM), while the distance in *c(3)G*$^{cc\Delta 1}$ mutants was reduced to 67.8 nm (±0.1 nm SEM)
167 (Fig 2.1C). The decrease in SC width is might be explained by the decreased length of
168 C(3)G due to the 213 amino acids that were deleted. Because a single amino acid
169 residue in a helix is predicted to be 0.15 nm in length, one would expect the decrease in
170 length of a single C(3)G$^{cc\Delta 1}$ homodimer to be 32 nm. Therefore, the width of the SC
171 (which contains C(3)G homodimers arranged in a head to head orientation) would be
172 predicted to be reduced by 64 nm in *c(3)G*$^{cc\Delta 1}$ mutants. Although the observed 50 nm
173 decrease in the width of the SC is less than expected, the difference may be due to

174 differences in the way that the C(3)G$^{cc\Delta 1}$ homodimer interacts with the oppositely
175 oriented homodimer emanating from the other lateral element. Most importantly, the
176 reduction in coiled-coil length created by removal of a large portion of the coiled-coil
177 domain does not disrupt the formation of tripartite SC, as is illustrated by the two lateral
178 tracks of C(3)G and the single track of Corolla observed using STED (Fig 2.1C,D).
179

180 **Loss of SC maintenance in early-mid pachytene is correlated with a reduction in**
181 ***X* chromosome crossing over**

182 The progressive (or temporal) loss of SC in *c(3)G$^{cc\Delta 1}$* flies allowed us to determine
183 whether or not the perdurance of full-length SC until early-mid pachytene was required
184 for proper crossing over and/or crossover placement. We examined recombination on
185 the *X* chromosome and found that the total amount of recombination along the entire
186 chromosome was decreased from 63 cM to 11.8 cM (Fig 3A, Table 1). This reduction in
187 exchange was clearly polar, a well-known attribute of recombination-deficient mutants in
188 *Drosophila* (Baker and Hall, 1976). Specifically, the chromosomal region distal and
189 medial to the centromere from *scute (sc)* to *vermillion (v)* exhibited a very low level of
190 crossing over (3.7% of wild type) while the centromere-proximal region from *v* to *yellow^{+}*
191 *(y^{+})* was only reduced to 31.3% of wild type (Fig 3A, Table 1).

192 The analysis of crossing over on the *3rd* chromosome did not reveal a reduction
193 in total map length when comparing wild type and *c(3)G$^{cc\Delta 1}$* flies (Fig 3B, Table 2, 50.9
194 cM and 64.4 cM respectively). However, the pattern of exchange was again altered in a
195 polar fashion, with a decrease in distal recombination between *roughoid (ru)* and *hairy*

196 *(h)* (Fig 3B, Table 2, 58.2% of wild type) and a large increase (to 447% of wild type) in
197 the centromere-proximal region between *scarlet (st)* and *curled (cu)* (Fig 3B, Table 2).
198 To ensure the *3rd* chromosome recombination phenotype was representative of
199 both large autosomes, we examined recombination on the *2nd* chromosome. As shown
200 in Fig 3.1 and Table 3, the effect of the $c(3)G^{cc\Delta 1}$ deletion on *2nd* chromosome
201 recombination mirrored that observed for the *3rd* chromosome with a decrease in distal
202 recombination and a large increase on centromere-proximal exchange (Fig 3.1, Table
203 3). The greater than 300% increase in recombination across the centromere-proximal
204 region on both the *2nd* and *3rd* chromosomes suggests that normal, full-length SC in
205 early-mid and mid pachytene is regulating, directly or indirectly, crossover placement
206 along the length of the chromosome.
207 The striking difference in recombination patterns between the *X* chromosome
208 and autosomes suggest that the *X* chromosome responds differently to aberrations in
209 the SC in early-mid pachytene than the autosomes. Such chromosome-specific defects
210 in recombination have not been previously documented in *Drosophila* (Hughes et al.,
211 2018; Parry and Sandler, 1974).
212
213 **Smaller in-frame deletions within the putative coiled-coil domain also cause a**
214 **loss of SC maintenance**
215 One potentially confounding factor in the analysis of the $c(3)G^{cc\Delta 1}$ mutants was the
216 decrease in the width of the SC (Fig 2.1C) caused by the removal of a large region of
217 the coiled-coil domain. The deletion of such a large region of the coiled coil could
218 change the ability of the C(3)G protein to interact with itself and form stable SC but it

219 might also remove sites important for interacting with other proteins. Therefore, in an
220 attempt to separate the multiple phenotypes seen in *c(3)G*$^{cc\Delta 1}$ flies, we created two
221 smaller deletions within the larger deletion, *c(3)G*$^{cc\Delta 2}$ (D346-T361) and *c(3)G*$^{cc\Delta 3}$ (K465-
222 V471) (Fig 4A). These smaller regions should not significantly affect the length of the
223 C(3)G protein based on the small number of amino acids deleted. These sites were
224 picked based on regions of C(3)G where the COILS score (Lupas et al., 1991) dipped
225 suggesting a loss of coiled-coil structure (Fig 4.1A). We hypothesized these might be
226 regions important for regulation of SC structure and/or function, independent of SC
227 width.

228 When SC formation in *c(3)G*$^{cc\Delta 2}$ and *c(3)G*$^{cc\Delta 3}$ mutants were examined by Corolla
229 staining, *c(3)G*$^{cc\Delta 2}$ flies displayed a similar SC length to wild type in early and early-mid
230 pachytene, but displayed a decrease in total SC length in mid pachytene when
231 compared to wild type (Fig 4B,C, $p=0.002$). However, *c(3)G*$^{cc\Delta 3}$ mutants never formed
232 fully assembled full-length SC (Fig 4B,C, $p<0.0001$). Although each of these deletions is
233 much smaller than the *c(3)G*$^{cc\Delta 1}$ deletion, *c(3)G*$^{cc\Delta 2}$ mutants did not display a loss of SC
234 length until mid pachytene, while *c(3)G*$^{cc\Delta 3}$ mutants had a more severe loss of SC in
235 early pachytene compared to *c(3)G*$^{cc\Delta 1}$ mutants (Fig 2B and 4B). We confirmed through
236 antibody staining that the SC that did assemble in *c(3)G*$^{cc\Delta 2}$ and *c(3)G*$^{cc\Delta 3}$ mutants
237 contained C(3)G (Fig 4.1B,C) in addition to Corolla (Fig 4B). The drastic differences in
238 SC formation and maintenance observed in these mutants gave us a tool to examine
239 the requirement of SC in early pachytene vs mid pachytene without the removal of a
240 large structural region of C(3)G.
241

242 **Full-length SC in mid pachytene is not necessary for *X* recombination**

243 When compared to *c(3)G*$^{cc\Delta 1}$ flies, the *c(3)G*$^{cc\Delta 2}$ mutants exhibited very different
244 recombination phenotypes. First, *c(3)G*$^{cc\Delta 2}$ mutants had relatively normal levels of
245 recombination along the *X* chromosome (109% of wild type, Table 1, Fig 5A) but still
246 displayed increased centromere-proximal recombination on the *3rd* chromosome in the
247 *st-cu* interval (347% of wild type, Table 2,Fig 5C). Centromere-distal recombination
248 between *ru-h* on the *3rd* chromosome was reduced to 65.5% of wild type levels in
249 *c(3)G*$^{cc\Delta 2}$ (Fig 5C, Table 2).

250 In contrast to *c(3)G*$^{cc\Delta 2}$, the *c(3)G*$^{cc\Delta 3}$ deletion greatly reduced recombination on
251 the *X* chromosome to 4.5% of wild type (Fig 5B, Table 1). This reduction was similar to,
252 but more severe than, the reduction in *X* recombination seen in *c(3)G*$^{cc\Delta 1}$ mutants
253 (18.7% of wild type, Table 1, Fig 3A). Additionally, *c(3)G*$^{cc\Delta 3}$ mutants mimicked the *3rd*
254 chromosome recombination pattern we saw in *c(3)G*$^{cc\Delta 1}$ and *c(3)G*$^{cc\Delta 2}$ (Fig 3B, Fig 5C,
255 Table 2) with a centromere-distal reduction and a large centromere-proximal increase in
256 recombination (Fig 5D, distal = 25.5% of wild type, proximal = 404% of wild type). These
257 large increases in proximal exchange parallel those observed in *c(3)G*$^{cc\Delta 1}$ mutants for
258 both the *2nd* and *3rd* chromosomes. We note that in all cases the mutant and control
259 crosses carry identical pericentromeric regions and therefore the observed effects on
260 exchange in the centromere-proximal regions of the autosomes cannot be attributed to
261 unrelated structural changes (See Methods).

262

263 **DSB formation in *c(3)G*$^{cc\Delta 1}$, *c(3)G*$^{cc\Delta 2}$, and *c(3)G*$^{cc\Delta 3}$ mutants**

264 To confirm that the decreases in *X* chromosome recombination observed in both the
265 *c(3)G*$^{cc\Delta 1}$ and *c(3)G*$^{cc\Delta 3}$ mutants were not due to a large decrease in the formation of
266 DSBs, we assessed DSB formation using γH2AV, a phosphorylated form of the histone
267 variant H2AV that specifically marks sites of DSBs. Although both *c(3)G*$^{cc\Delta 1}$ and
268 *c(3)G*$^{cc\Delta 3}$ flies exhibited normal kinetics for DSB repair from early to mid pachytene,
269 *c(3)G*$^{cc\Delta 1}$ flies (but not *c(3)G*$^{cc\Delta 3}$ flies) displayed a decrease in the number of DSBs
270 formed in early pachytene (Fig 5.1A, p=0.03). Because *X* chromosome recombination
271 was more severely affected in *c(3)G*$^{cc\Delta 3}$ flies compared to *c(3)G*$^{cc\Delta 1}$ flies, we do not
272 believe the early pachytene decrease in *c(3)G*$^{cc\Delta 1}$ mutants is biologically relevant to the
273 decrease in crossing over on the *X* chromosome. Lastly, we assessed DSB formation in
274 *c(3)G*$^{cc\Delta 2}$ flies and saw a slight decrease in the number of DSBs formed in early
275 pachytene compared to wild type (Fig 5.1A, p=0.006). However, since *c(3)G*$^{cc\Delta 2}$ flies did
276 not have an overall decrease in the formation of crossovers, the decrease in γH2AV
277 may not be biologically significant.

278 One possible explanation for the increase in centromere-proximal recombination
279 might be the induction of ectopic DSBs within the heterochromatin that were not
280 induced by Spo11. To confirm that the centromere-proximal recombination was due to
281 Spo11 breaks, we constructed a double mutant with *c(3)G*$^{cc\Delta 3}$ and *vilya*^{826}, a
282 recombination nodule component that is necessary for the induction of Spo11-induced
283 breaks (Lake et al., 2015). When we assessed *3rd* chromosome recombination we saw
284 very low levels of recombination (total map length = 1.4 cM, Fig 5.1B), similar to the
285 recombination seen in *vilya*^{826} alone (Lake et al., 2015). This confirmed that the

286 crossovers in *c(3)G*$^{cc\Delta 3}$ mutants are due to programmed Spo11 DSBs and not an
287 increase in DNA damage.
288
289 **Chromosome segregation in *c(3)G*$^{cc\Delta 1}$, *c(3)G*$^{cc\Delta 2}$, and *c(3)G*$^{cc\Delta 3}$ mutants**
290 All previously characterized mutants in *Drosophila* that are unable to form crossovers,
291 or have a significant reduction in crossovers genome-wide, display high levels of both *X*
292 and *4th* chromosome nondisjunction (Collins et al., 2014; Krishnan et al., 2014;
293 Manheim and McKim, 2003; Page and Hawley, 2001; Yan and McKee, 2013). The high
294 levels of *X* nondisjunction observed in these recombination-defective mutants involves
295 the interactions between both non-crossover *X* chromosomes and non-crossover
296 autosomes (Baker and Hall, 1976; Hughes et al., 2018), such that two *X* chromosomes
297 segregate from one autosome with the remaining autosomes segregating at random. In
298 the absence of non-crossover autosomes, non-crossover *X* chromosomes will
299 segregate normally.
300 When the rate of missegregation of the *X* and *4th* chromosomes was assessed in
301 all three mutants, neither *c(3)G*$^{cc\Delta 1}$ or *c(3)G*$^{cc\Delta 2}$ mutants showed significantly increased
302 levels of *X* or *4th* chromosome nondisjunction when compared to wild type (Table 4).
303 *c(3)G*$^{cc\Delta 3}$ mutants displayed low levels of *X* (4.5%) and *4th* (2.0%) non-disjunction (Table
304 4). However, this low level of non-disjunction is much lower than the 39.2% reported in
305 *c(3)G* null mutants where the SC is completely absent (Hall, 1972).
306 The absence of an observed increase in *X* nondisjunction in *c(3)G*$^{cc\Delta 1}$ and
307 *c(3)G*$^{cc\Delta 2}$ mutants is most likely explained by the absence of the nonexchange
308 autosomes required to induce *X* chromosome nondisjunction. However, the low levels

309 of *X* nondisjunction observed in *c(3)G*$^{cc\Delta 3}$ mutants might also be compatible with a
310 proposed role for C(3)G-like proteins in mediating achiasmate segregations (Gladstone
311 et al., 2009; Previato de Almeida et al., 2019). Therefore, the severe SC fragmentation
312 present in *c(3)G*$^{cc\Delta 3}$ mutants may cause a mild segregation defect even in the presence
313 of autosomal recombination.
314

315 **The loss of full-length SC in these mutants parallels the decrease in euchromatic**
316 **homolog pairing**

317 Homolog pairing is reduced in mutants lacking SC (Gong et al., 2005; Page et al., 2008;
318 Sherizen et al., 2005). Thus, since our mutants exhibit SC defects in early to mid
319 pachytene, we utilized them to investigate the importance of full-length SC in the
320 maintenance of homolog pairing in *Drosophila*. Fluorescence In Situ Hybridization
321 (FISH) was used to examine homologous pairing, and to mark the distal and proximal
322 loci of the *X* chromosome.

323 In wild type, 90% to 100% of the *X* chromosome was paired from early to mid
324 pachytene (Fig 6A). To determine what the baseline level of pairing is in the absence of
325 the SC, *X* chromosome pairing was assessed in females homozygous for a null allele of
326 *c(3)G* (*c(3)G*^{68}). In this genotype the centromere-distal region of the chromosome was
327 most affected, with an average of 37% paired between early and early-mid pachytene,
328 while the centromere-proximal region was paired in about half the nuclei (Fig 6.1A,
329 51.5%).

330 Starting at early-mid pachytene *c(3)G*$^{cc\Delta 2}$ mutants exhibited a slight pairing defect
331 at the centromere-distal locus of the *X* chromosome (Fig 6A, early= 90.9%, early-mid

332 pachytene= 75%, mid pachytene= 58.8%) but were relatively well-paired at the
333 centromere-proximal locus (Fig 6A, early=93.9%, early-mid pachytene= 95%, mid
334 pachytene= 88.2%). Both *c(3)G*$^{cc\Delta 1}$ and *c(3)G*$^{cc\Delta 3}$ mutants displayed a progressive loss
335 of pairing at both proximal and distal loci on the *X* chromosome. *c(3)G*$^{cc\Delta 1}$ mutants had
336 almost a complete loss of distal pairing by mid pachytene while *c(3)G*$^{cc\Delta 3}$ mutants only
337 maintained 26% pairing (Fig 6A).

338 These abnormalities in pairing maintenance correspond well with the
339 recombination pattern seen on the *X* chromosome in *c(3)G*$^{cc\Delta 1}$ and *c(3)G*$^{cc\Delta 3}$ mutants in
340 the sense that the distal region of the *X* chromosome was more affected than the
341 proximal regions (Fig 3A and 6A). The centromere-distal decrease in recombination on
342 the *3rd* chromosome in *c(3)G*$^{cc\Delta 1}$ and *c(3)G*$^{cc\Delta 3}$ mutants is displayed in conjunction with
343 a similar loss of pairing. We examined pairing at distal, medial, and proximal loci on the
344 *3rd* chromosome throughout pachytene. Similar to the *X* chromosome, both *c(3)G*$^{cc\Delta 1}$
345 and *c(3)G*$^{cc\Delta 3}$ mutants displayed a similar trend of reduced pairing of the *3rd*
346 chromosome, with a progressive decrease in centromere-distal pairing that mirrors the
347 recombination data (Fig 6B). The medial and proximal region of the *3rd* chromosome
348 remained relatively paired from early to mid pachytene (Fig 6B). It should be noted that
349 in *c(3)G*^{68} null mutants pairing on the *3rd* chromosome was more strongly reduced;
350 however, the proximal region (45% paired) was still paired more frequently than was the
351 distal region (35% paired) (Fig 6.1A).

352 To confirm that the loss of distal pairing on the *3rd* chromosome observed in
353 *c(3)G*$^{cc\Delta 1}$ and *c(3)G*$^{cc\Delta 3}$ mutants was representative of the autosomes, we also
354 examined pairing on the *2nd* chromosome in *c(3)G*$^{cc\Delta 1}$ mutants. Pairing on the *2nd*

355 chromosome mirrored that of the *3rd* chromosome with a progressive loss of distal
356 pairing but very little effect on medial and proximal pairing (Fig 6.1B). The significant
357 loss of distal pairing might explain why there are stronger recombination defects in the
358 distal regions of both the *X* and *3rd* chromosomes in $c(3)G^{cc\Delta 1}$ and $c(3)G^{cc\Delta 3}$ flies. By
359 the same reason, the autosomal pairing that is maintained in these mutants is proximal,
360 which may allow for an increased number of recombination events that are proximal to
361 the centromere.
362
363 **Centromere pairing in meiosis is not affected in the absence of full-length SC**
364 In wild type *Drosophila* females, the eight centromeres (two for each of the four
365 chromosomes) pair in the pre-meiotic cysts and then cluster into an average of two
366 clusters by early pachytene (Takeo et al., 2011). The SC is important for centromere
367 clustering in early meiotic cells with an average of four clusters in *c(3)G, cona* and
368 *corolla* null mutants (Collins et al., 2014; Takeo et al., 2011; Tanneti et al., 2011). Using
369 an antibody against CID, a centromere specific histone, we assessed if centromere
370 clustering was altered in the context of SC loss in early to mid pachytene.
371 Oocytes from both wild type, $c(3)G^{cc\Delta 1}$, and $c(3)G^{cc\Delta 2}$ flies contained an average
372 number of clusters from 1.7 to 2.5 foci in early to mid pachytene (Fig 6.2A,B). $c(3)G^{cc\Delta 1}$
373 mutants did display significantly more clusters than controls in early and mid pachytene
374 (Fig 6.2A, p= 0.01 and 0.002 respectively). However, because the average was 2.5 foci,
375 the loss of SC is not likely to be impacting centromere pairing in $c(3)G^{cc\Delta 1}$. $c(3)G^{cc\Delta 3}$
376 mutants had an average of 3.6 clusters in all three stages (Fig 6.2B, p< 0.001),

377 suggesting that SC assembly defects in early pachytene may be sufficient to disrupt
378 centromere clustering but not centromere pairing.
379

380 ## Discussion

381 The SC plays multiple roles during meiosis that illustrate its importance in ensuring the
382 successful transmission of genetic information from one generation to the next, yet our
383 knowledge of how the SC is involved in regulating meiotic processes, such as
384 recombination and the maintenance of pairing, is limited due to the integral nature of
385 each SC component. Here we report the first partial loss-of-function SC mutations in a
386 central region component in *Drosophila*. We use the different stages of SC loss found in
387 these mutants to show there is a temporal requirement of the SC in the regulation of
388 crossover number and placement on the *X* chromosome versus the autosomes (Fig 7).
389 Additionally, full-length SC is important for maintaining euchromatic homolog pairing in
390 distal chromosomal regions.
391

392 **Regulation of SC assembly and disassembly**

393 Both the regulation of SC assembly and disassembly, and it's maintenance after
394 assembly, is poorly understood. Work in other organisms has shown that post-
395 translational modifications are important in SC structure and function. It is known that
396 SUMOylation promotes assembly of the SC while phosphorylation promotes
397 disassembly of the SC with modifications occurring on multiple SC proteins (Jordan et
398 al., 2012; Nadarajan et al., 2017; Sato-Carlton et al., 2017). Thus far, no post-
399 translationally modified sites have been identified on C(3)G. However, it is likely that

400 these sites do exist, and we speculate that sites promoting SC assembly, maintenance,
401 and disassembly may be disrupted in these mutants.
402 Another possibility is that the deletions described here could destabilize protein-
403 protein interaction sites between C(3)G and other central region proteins resulting in
404 unstable SC that is difficult to maintain. We note that the mutant with the smallest
405 deletion, *c(3)G*$^{cc\Delta 3}$, exhibited the strongest SC defect. While this deletion was predicted
406 to only disrupt a single coil, the best explanation for the more severe phenotype is that it
407 actually disrupts the coiled-coil. This may have caused a large disruption in the rest of
408 the coiled-coil structure. In the future, it will be important to further dissect these
409 domains to better understand the regulation of SC assembly and disassembly.
410
411 **A role for the SC in the maintenance of homolog pairing**
412 A surprising result from these studies was the ability of these deletions to allow the
413 progressive loss of homologous euchromatic pairing through pachytene. The
414 mechanism behind establishing and maintaining homolog pairing is a long-standing,
415 unanswered question in the meiosis field. Previous work in *Drosophila* has shown that
416 in the complete absence of the central region proteins C(3)G and CONA, euchromatic
417 pairing is significantly reduced in early-mid and mid pachytene (Gong et al., 2005; Page
418 et al., 2008; Sherizen et al., 2005).
419 Our partial loss-of-function mutations have allowed us to test the importance of
420 C(3)G in maintaining pairing throughout pachytene when SC is present in early
421 pachytene (unlike previous studies of null mutants in which the SC is always absent).
422 From these mutants we now have a time line of when the SC is necessary to maintain

423 pairing and recombination on the *X* chromosome and the autosomes. By comparing
424 these mutants, we can hypothesize that the *X* chromosome needs full-length SC earlier
425 in pachytene for proper maintenance of pairing and recombination while the autosomes
426 are likely capable of placing crossovers as late as mid pachytene resulting in a
427 centromere-proximal shift in crossovers where pairing is maintained (Fig 7).

428 In both $c(3)G^{cc\Delta 1}$ and $c(3)G^{cc\Delta 3}$ mutants, distal pairing of the *X* chromosome and
429 the autosomes was most strongly reduced. One likely explanation for this is that
430 normally the disassembly of the SC is initiated on the euchromatic chromosome arms
431 with the centromeric region being removed last. Since the loss of the SC in $c(3)G^{cc\Delta 1}$
432 and $c(3)G^{cc\Delta 3}$ mutants occurs in a manner similar to wild type SC disassembly, the distal
433 regions of the chromosome may be affected earlier and more strongly than the
434 centromere-proximal regions. The centromere-proximal region contains a large amount
435 of heterochromatin that could be mediating pairing interactions and stabilizing pairing in
436 the absence of the SC (Dernburg et al., 1998). Furthermore, our examination of
437 centromere pairing suggests that the centromeres are still paired (Fig 6.2) and could be
438 facilitating the centromere-proximal pairing. This idea is supported by the higher levels
439 of centromere-proximal pairing compared to distal pairing in $c(3)G^{68}$ (Fig 6.1A).

440 Finally, we speculate that the ability of the $c(3)G^{cc\Delta 1}$ mutants to exhibit a
441 centromere-distal pairing defect that is more severe than the defect seen in $c(3)G^{68}$
442 mutants results from the residual proximal crossovers that do form in $c(3)G^{cc\Delta 1}$ mutants.
443 Previous work has shown that crossovers can preserve synapsis but only in their vicinity
444 (Maguire, 1985; Maguire and Riess, 1994). Perhaps the stresses that provoke
445 separation become more concentrated on the distal regions that lack crossovers. For

446 example, it is possible that the un-tethered distal regions could experience a higher
447 mechanical stress due to nuclear movements than the pericentric regions containing a
448 crossover. The lack of a strong pairing defect in *c(3)G*$^{cc\Delta 2}$ mutants is probably due to
449 the persistence of full-length SC until mid pachytene. Together these data support a role
450 for the SC in maintaining euchromatic pairing during early to mid prophase (Fig 7).
451

452 **What causes the increase in centromere-proximal recombination events?**

453 The autosomal increase in centromere-proximal crossovers displayed in these mutants
454 mimics the interchromosomal effect (Crown et al., 2018; Joyce and McKim, 2009). The
455 interchromosomal effect has been reported in flies that are heterozygous for
456 chromosomes aberrations that suppress exchange in trans to a wild type chromosome
457 (Lucchesi et al., 1976). Thus the absence of crossover formation on one chromosome
458 promotes increased recombination on the other chromosomes, with more crossovers
459 placed in the centromere-proximal regions (Crown et al., 2018; Joyce and McKim,
460 2009). The mechanism that controls the interchromsomal effect in balancer
461 heterozygotes is poorly understood. It is possible that the interchromosomal effect is
462 partially responsible for the increase in centromere-proximal crossovers in *c(3)G*$^{cc\Delta 1}$ and
463 *c(3)G*$^{cc\Delta 3}$ mutants due to the loss of *X* chromosome recombination.

464 However, the interchromosomal effect cannot explain the increase in
465 centromere-proximal recombination in *c(3)G*$^{cc\Delta 2}$ mutants since *X* recombination appears
466 normal. Another explanation for the increase in centromere-proximal recombination
467 events may be the premature loss of the SC at distal regions of the chromosome. It is
468 unknown how much of a role the SC plays in the repair of DSBs into crossover versus

469 non-crossover events. It is possible the SC must be present to interact with factors
470 necessary for regulating the placement of crossovers. For example, Vilya, a pro-
471 crossover factor, localizes to the SC and DSBs prior to being recruited to recombination
472 nodules (Lake et al., 2015). If DSB repair on the autosomes does not occur until early-
473 mid pachytene and the SC is necessary for the determination of a crossover fate, it
474 follows that distal loss of SC would result in a shift of crossover formation towards
475 centromere-proximal regions where the SC is still present. This mechanism could also
476 be increasing centromere-proximal recombination in *c(3)G*$^{cc\Delta 1}$ and *c(3)G*$^{cc\Delta 3}$ flies.
477 Alternatively, SC-independent heterochromatic pairing may be holding the centromere-
478 proximal region in close proximity allowing for crossing over in that region. In addition to
479 interacting with pro-crossover factors the SC may be interacting with a currently
480 unknown protein which regulates crossover placement differently on the *X* chromosome
481 versus the autosomes.
482
483 **Why is there a difference between the *X* chromosome and the autosomes?**
484 This set of mutants represents a unique tool to investigate not only the temporal
485 requirements of the SC but the differences in crossover placement between the *X*
486 chromosome and the autosomes. Since *c(3)G*$^{cc\Delta 2}$ mutants do not display defects in *X*
487 chromosome recombination we conclude that full-length SC in early-mid pachytene is
488 necessary for *X* chromosome crossover placement (Fig 7). Examining autosomal
489 recombination in all three mutants suggests that full-length SC is necessary in mid
490 pachytene for proper crossover distribution on the autosomes (Fig 7). There are multiple

491 explanations for the recombination differences between the *X* chromosome and the
492 autosomes.
493 The first of these hypotheses is that there might exist a timing difference in either
494 synapsis or crossover placement between the *X* chromosome and the autosomes. Work
495 in *C. elegans* has provided evidence for timing differences between the sex
496 chromosomes and the autosomes. For example, the *X* chromosome initiates pre-
497 meiotic DNA replication later than the autosomes (Jaramillo-Lambert et al., 2007;
498 Mlynarczyk-Evans and Villeneuve, 2017). Additionally, in *C. elegans* the *X* chromosome
499 and the autosomes pair at the same time but synapsis of the *X* chromosome is delayed
500 compared to the autosomes (Mlynarczyk-Evans and Villeneuve, 2017). The timing of
501 when each chromosome is fully synapsed could be critical to ensure normal crossover
502 placement, and the premature disruption of synapsis may affect the activity of pro-
503 crossover factors. For example in *C. elegans*, the XND-1 protein is required for
504 genome-wide crossover placement and is important for normal rates of DSBs on the *X*
505 chromosome (Wagner et al., 2010). Currently, it is unknown in *Drosophila* if there are
506 differences in the timing of DSB repair or synapsis of the *X* chromosome as compared
507 to the autosomes, and our data suggest this as a possibility.
508 A second, but not mutually exclusive, explanation for the differences between the
509 chromosomes may be a structural one. The *X* chromosome is acrocentric (centromere
510 is near the end of the chromosome), while the autosomes are both metacentric
511 (centromere is near the center of the chromosome), and perhaps, these structural
512 differences mean that the *X* chromosome is more sensitive to loss of the SC. Our data
513 suggest that loss of SC maintenance disrupts the maintenance of euchromatic homolog

514 pairing more severely on the *X* chromosome than on the autosomes. It is unknown if
515 metacentric chromosomes are different in terms of synapsis and recombination as
516 compared to acrocentric chromosomes, and further investigation is needed to determine
517 if structural differences affect these processes.

518 It is clear from decades of research that the regulation of recombination requires
519 many factors and precise timing. Here we show that the SC plays a vital role in
520 maintaining homolog pairing and proper crossover distribution in *Drosophila* female
521 meiosis. Many differences between sex chromosomes and autosomes have been
522 documented in a multitude of organisms, and our data are consistent with these
523 differences extending into the processes that control chromosome pairing and
524 recombination. With this set of mutants, we have established a new system to examine
525 *X* chromosome and autosome biology in *Drosophila* meiosis that will allow future work
526 to unravel the mechanism behind meiotic chromosomal differences.

527

528 Materials and Methods

529 *Stocks*

530 *Drosophila* stocks were maintained on standard food at 24°C. Descriptions of genetic
531 markers and chromosomes can be found at http://www.flybase.org/. Wild type refers to
532 the genotype: *y w; +/+; +/+; sv*$^{spa\text{-}pol}$, unless stated otherwise. The key resource table
533 contains a list of all the fly stocks used in this manuscript.

534

535 *Construction of c(3)G*$^{cc\Delta 1}$ *mutants*

536 To aid in screening for *c(3)G*$^{cc\Delta 1}$ mutant flies, we incorporated a *piggyBac*
537 transposon carrying a *3xP3*-DsRed that expresses in the fly eye into the intron directly
538 downstream of the intended *c(3)G*$^{cc\Delta 1}$ deletion [intron 5 of *c(3)G*] in the homologous
539 repair template plasmid. Repair of the Cas9-induced DSB using the homologous repair
540 plasmid will insert the desired mutation and the *piggyBac* transposon into the genome at
541 the *c(3)G* locus. This allowed us to screen for the flies that undergo DSB repair off the
542 homologous repair plasmid by searching for those that express dsRed in the eyes.
543 Then, after isolation and confirmation of the desired *c(3)G* mutation, we excised the
544 *piggyBac* transposon by crossing in a transposase. This removed any potential effect
545 the *piggyBac* transposon may have on the expression of *c(3)G*.
546 The *piggyBac* transposon plasmid was constructed to have flanking *Aar*I and
547 *Sap*I restriction sites (Addgene 51434). We used PCR to obtain two fragments of *c(3)G*
548 from the *Drosophila* genome that flanked the position where the *piggyBac* would be
549 inserted and added in either an *Aar*I or *Sap*I restriction site. The ~2600-bp fragment
550 upstream of the *piggyBac* insertion site contained *Aar*I sites and was obtained using
551 these primers: Forward, tataCACCTGCattaCCGAcgctagtggctcctagagttcag; Reverse,
552 gcagCACCTGCgcggTTAAtgaaaaagaatttataagtcttaccattaggttatc. The ~1000-bp
553 fragment downstream of the *piggyBac* insertion site contained *Sap*I sites and was
554 obtained using these primers: Forward, gccgGCTCTTCNTAAcctttttctacaaaatgatttatt;
555 Reverse, gtatGCTCTTCNCGGtcatcaaaacatagtttagtatcg.
556 To insert these fragments into the *piggyBac* plasmid, the plasmid and the
557 downstream *Sap*I-containing PCR was digested with *Sap*I (also called *Lgu*I from
558 ThermoFisher, ER1931), phosphatase treated (Antarctic phosphatase, NEB M0289S),

559 and ligated together using T4 ligase (NEB, M0202S). Then, to make the *c(3)G*$^{cc\Delta 1}$
560 mutation, the upstream *Aar*I-containing PCR fragment was TOPO cloned using the Zero
561 Blunt TOPO kit (ThermoFisher, 451245) and cut using the restriction enzyme *HindIII*
562 (NEB, R0104S) to remove the 702-bp fragment from *c(3)G* creating the *c(3)G*$^{cc\Delta 1}$
563 mutation. The cut TOPO *AarI* plasmid was then phosphatase treated and ligated back
564 together to create the *c(3)G*$^{cc\Delta 1}$ deletion. Then, this plasmid was digested with AarI
565 (ThermoFisher ER1581) to generate a ~1900-bp fragment containing the *c(3)G*$^{cc\Delta 1}$
566 deletion, which was cloned into the *piggyBac* plasmid containing the downstream *Sap*I
567 *c(3)G* fragment. This created the *c(3)G*$^{cc\Delta 1}$ homologous repair template plasmid, which
568 was fully sequenced to ensure all cloning occurred in the correct direction (See Key
569 Resources for primers).

570 A CRISPR target sequence was selected from the flyCRISPR Optimal Target
571 Finder (http://tools.flycrispr.molbio.wisc.edu/targetFinder/). Only a single site upstream
572 of the *c(3)G*$^{cc\Delta 1}$ deletion was selected (AAAGCTTTGTTGGCCTGTATTGG) and
573 constructed into the pU6-BbsI-chiRNA guide RNA (gRNA) plasmid (Addgene 45946).
574 Sense (CTTCGAAAGCTTTGTTGGCCTCTAT) and antisense
575 (AAACATAGAGGCCAACAAAGCTTTC) oligonucleotides were ordered from IDT and
576 cloned into the gRNA plasmid as described by the flyCRISPR subcloning pU6-gRNA
577 protocol (http://flycrispr.molbio.wisc.edu/protocols/gRNA). After selection of the CRISPR
578 target sequence, three single nucleotide polymorphisms (SNPs) were made in the
579 CRISPR target sequence (the mutated bases are shown in bold:
580 ccaataga**a**gc**g**aa**t**aaagcttt) in the *c(3)G*$^{cc\Delta 1}$ homologous repair template plasmid to
581 prevent Cas9 from cutting this plasmid. These SNPs were made using the Quik Change

582 II XL Site-Directed Mutagenesis Kit (Agilent Technology, 200521). The gRNA and
583 *c(3)G*$^{cc\Delta 1}$ homologous repair template plasmid were sent to Genetivision (Houston,
584 Texas) for injection into *y m[VASA-Cas9-3xGFP]ZH-2A-3xRFP w*^{1118}*/FM7c* flies (BLM
585 51323). Genetivision injected the gRNA plasmid at 250 ng/µl and the *c(3)G*$^{cc\Delta 1}$
586 homologous repair template at 500 ng/µl.

587 *c(3)G*$^{cc\Delta 1}$ was isolated by crossing the G0 injected flies to *y w; Pr/TM3; sv*$^{spa\text{-}pol}$,
588 then the F1 progeny were screened for expression of dsRed in the fly eyes. Due to the
589 *VASA-Cas9* transgene also being marked with RFP, only F1 males could be screened
590 for CRIPSR insertion using dsRed expression. 15 G0 males were recovered from the
591 commercially injected embryos (Genetivision) and crossed to *y w; Pr/TM3; sv*$^{spa\text{-}pol}$. PCR
592 and Sanger sequencing were used to confirm that that male had repaired off the repair
593 template to incorporate the *c(3)G*$^{cc\Delta 1}$ deletion mutation at the genomic *c(3)G* locus (See
594 Key Resources). This was done by using forward and reverse primers that were outside
595 of the 1kb both up and downstream repair sequence (See Key Resources). Following
596 removal of the *piggyBac,* we sequenced the entire *c(3)G* gene to confirm both the
597 precise excision of the transposon and that the only lesion in the gene was the desired
598 *c(3)G*$^{cc\Delta 1}$ deletion mutation. Only one male was identified and was used to establish a
599 stock.

600

601 *Construction of c(3)G*$^{cc\Delta 2}$ and *c(3)G*$^{cc\Delta 3}$ *mutants*

602 A CRISPR target sequence was selected from the flyCRISPR Optimal Target Finder
603 (http://tools.flycrispr.molbio.wisc.edu/targetFinder/). Two guide RNAs were created for
604 *c(3)G*$^{cc\Delta 2}$ and *c(3)G*$^{cc\Delta 3}$ (guide 1 *c(3)G*$^{cc\Delta 2}$: GCTCAATGCGATC**T**TC**A**AGCTG**G**, guide 2

605 *c(3)G*$^{cc\Delta 2}$: GATTGACTGATCA**G**GC**A**AC**G**AG**G**, guide 1 *c(3)G*$^{cc\Delta 3}$:
606 GCTCTTCCTG**A**TTGCTGCG**A**TG**G**, and guide 2 *c(3)G*$^{cc\Delta 3}$:
607 TCTTGAACAAC**A**ATCTGTC**A**AG**G**) and constructed into the pU6-BbsI-chiRNA guide
608 RNA (gRNA) plasmid (Addgene 45946). Sense and antisense oligonucleotides (guide 1
609 *c(3)G*$^{cc\Delta 2}$: CTTCGCTCAATGCGATCTTCAAGCTGG,
610 AAACCCAGCTTGAAGATCGCATTGAGC; guide 2 *c(3)G*$^{cc\Delta 2}$:
611 CTTCGATTGACTGATCAGGCAACGAGG, AAACCCTCGTTGCCTGATCAGTCAATC;
612 guide 1 *c(3)G*$^{cc\Delta 3}$: CTTCGCTCTTCCTGATTGCTGCGATGG,
613 AAACTCGCAGCAATCAGGAAGAGC; guide 2 *c(3)G*$^{cc\Delta 3}$:
614 CTTCTCTTGAACAACAATCTGTCAAGG, AAACTGACAGATTGTTGTTCAAGAC) were
615 ordered from IDT and cloned into the gRNA plasmid as described by the flyCRISPR
616 subcloning pU6-gRNA protocol (http://flycrispr.molbio.wisc.edu/protocols/gRNA).
617 The homologous repair constructs were created using the NEBuilder HiFi DNA
618 Kit (NEB, E5520S) and contained 1,000 bases upstream of the first guide RNA target
619 Cas9 site, the *c(3)G* sequence with either 42 bp (*c(3)G*$^{cc\Delta 2}$) or 21 bp (*c(3)G*$^{cc\Delta 3}$)
620 removed, and 1,000 bases downstream of the second guide RNA site. The PAM
621 sequences in the *c(3)G* gene were mutated using the Quik Change II XL Site-Directed
622 Mutagenesis Kit (Agilent Technology). The bases changed are in bold above.
623 Additionally, a restriction site was engineered into the repair template, without creating
624 coding changes, to aid in genotyping (*Spe*I for *c(3)G*$^{cc\Delta 2}$ and *Nhe*I for *c(3)G*$^{cc\Delta 3}$).
625 250 ng of each gRNA plasmid and 500 ng of the homologous repair template
626 plasmid were injected (BestGene) into *y nosCas9* (on *X* chromosome, BDSC #54591).
627 Potential CRISPR/Cas9 hits were screened with primers (See Key Resources), which

628 amplify a region spanning the deletion and were digested with either *Spe*I or *Nhe*I
629 allowing for visualization of heterozygotes. Once a CRISPR/Cas9 insertion was
630 identified, the entire *c(3)G* gene was sequenced to ensure the repair plasmid did not
631 insert.
632
633 *Nondisjunction and recombination assays*
634 To assay recombination along the *X* chromosome, females of the genotypes: (1) y^1 sc^1
635 cv^1 v^1 f^1 y^+/y w; $sv^{spa\text{-}pol}$; 2) y^1 sc^1 cv^1 v^1 f^1 y^+/y w; ru^1 h^1 $Diap1^1$ st^1 cu^1 $c(3)G^{cc\Delta 1}$ ca^1;
636 $sv^{spa\text{-}pol}$/+; 3) y^1 sc^1 cv^1 v^1 f^1 y^+/y w; ru^1 h^1 $Diap1^1$ st^1 cu^1 $c(3)G^{cc\Delta 2}$ ca^1; $sv^{spa\text{-}pol}$/+; 4) y^1
637 sc^1 cv^1 v^1 f^1 y^+/y w; ru^1 h^1 $Diap1^1$ st^1 cu^1 $c(3)G^{cc\Delta 3}$ ca^1; $sv^{spa\text{-}pol}$/+) were crossed to y^1 sc^1
638 cv^1 v^1 f^1 car^1/B^SY males. For *X* recombination analysis, only the female progeny were
639 analyzed for the intervals *sc-cv*, *cv-v, v-f, f-y+*.
640 To assay recombination along the *2nd* chromosome, females of the genotypes:
641 1) *y w/w;* net^1 dpp^{ho} dpy^{ov1} b^1 pr^1 cn^1/+; ru^1 h^1 $Diap1^1$ st^1 cu^1 $c(3)G^{cc\Delta 1}$ ca^1/ $c(3)G^{cc\Delta 1}$ ca^1;
642 $sv^{spa\text{-}pol}$/+; 2) w^+/yw; net^1 dpp^{ho} dpy^{ov1} b^1 pr^1 cn^1/+ were crossed to w^+/Y; net^1 dpp^{ho}
643 dpy^{ov1} b^1 pr^1 cn^1 males. For *2nd* recombination analysis, only the female progeny were
644 analyzed for the intervals *net-dpp, dpp-dpy, dpy-b, b-pr, pr-cn.*
645 To assay recombination frequency along the *3rd* chromosome females of the
646 following genotypes: 1) *y w/* w^+; ru^1 h^1 $Diap1^1$ st^1 cu^1 sr^1 e^s ca^1/+; 2) *y w/* w^+; ru^1 h^1
647 $Diap1^1$ st^1 cu^1 $c(3)G^{cc\Delta 1}$ ca^1/ $c(3)G^{cc\Delta 1}$ ca^1; $sv^{spa\text{-}pol}$/+; 3) *y w/*w^+; ru^1 h^1 $Diap1^1$ st^1 cu^1
648 $c(3)G^{cc\Delta 2}$ ca^1/ $c(3)G^{cc\Delta 2}$ ca^1; $sv^{spa\text{-}pol}$/+; 4) *y w/*w^+; ru^1 h^1 $Diap1^1$ st^1 cu^1 $c(3)G^{cc\Delta 3}$ ca^1/
649 $c(3)G^{cc\Delta 3}$ ca^1; $sv^{spa\text{-}pol}$/+; were crossed to *w+/Y;* ru^1 h^1 $Diap1^1$ st^1 cu^1 sr^1 e^s ca^1 males.

650 For *3rd* recombination analysis, only the female progeny were analyzed for the
651 intervals *ru-h, h-st, st-cu.*
652 To measure the rate of both *X* and *4*th chromosome nondisjunction single virgin
653 females of the indicated genotype were mated to multiple *X^Y, In(1)EN, v f B; C(4)RM,*
654 *ci ey*^{R} males. Calculations to determine the percentage of *X* and *4*th chromosome
655 nondisjunction were performed as previously described (Hawley et al., 1992; Zitron and
656 Hawley, 1989).
657
658 *Immunostaining of whole-mount ovaries*
659 Germarium preparation for whole-mount immunofluorescence was modified from the
660 protocol described in (Lake et al., 2015), with dissections performed in PBS with 0.1%
661 Tween (PBST). Primary antibodies used included affinity-purified rabbit anti-Corolla
662 (1:2000), mouse anti-C(3)G 1A8-1G2, 5G4-1F1, and 1G5-2F7 (all at 1:500), rabbit anti-
663 histone H2AVD pS137 (1:500) (Rockland Inc.), mouse anti-γH2AV (1:1000) (Iowa
664 Hybridoma Bank), rat anti-CID (used at 1:3000; gift from Claudio Sunkel), and rat anti-
665 CID (1:500) (Hanlon et al., 2018). All secondary antibodies were used at 1:500, and the
666 secondary antibodies used were Alexa Fluor 488 goat anti-mouse (ThermoFisher,
667 A11001), Alexa Fluor 555 goat anti-mouse (ThermoFisher, A21422), Alexa Fluor 647
668 goat anti-mouse (ThermoFisher, A21235), Alexa Fluor 488 goat anti-rabbit
669 (ThermoFisher, A11008), Alexa Fluor 555 goat anti-rabbit (ThermoFisher, A21428),
670 Alexa Fluor 647 goat anti-rat (ThermoFisher, A21434), and Alexa Fluor 555 goat anti-rat
671 (ThermoFisher, A21247).

672 For STED imaging, samples were imaged with 100x, N.A 1.40 oil. objective on a
673 Lieca SP8 Gated STED microscope. Alexa Flour 647 labeled secondary was imaged
674 with a pulsed white light (80 MHz) tuned to 647 nm; Alexa Fluor 594 labelled secondary
675 was imaged with the same white laser tuned at 594 nm. Both secondaries were
676 depleted with a pulsed STED 775 nm laser with 80-90% maximum power. All images
677 were acquired in 2D mode to improve lateral resolution, and each image was averaged
678 8 times in line average mode. The emission photons were collected with an internal
679 Leica HyD hybrid detector with a time gate between 1-6 ns. Raw STED images were
680 deconvolved with the STED module in Huygens professional deconvolution software
681 (version 14.10; Scientific Volume Imaging). A theoretical estimated point spread
682 function was calculated from the raw images metadata. We used the default setting to
683 process images, but the background was measured from raw data, also the signal to
684 noise was set in the range of 15-20 depending on the signal intensity.
685
686 *Fluorescent in situ hybridization*
687 FISH probes were designed from bacterial artificial chromosomes (BACs) obtained from
688 the Children's Hospital Oakland Research Institute (CHORI;
689 http://bacpacresources.org/library.php?id=30). The following BACs were used: for *2L*
690 RP98-28O9 (polytene band 22A2-22A4), RP98-43K24 (polytene band 32E2-32F2),
691 RP98-7D17 (polytene band 38E4-38F4); for *3L* RP98-2N23 (polytene band 61D-61E),
692 RP98-26C20 (polytene band 69B1-69C2), RP98-3J2 (polytene band 77F5-78B1); for
693 the *X* RP98-3D13 (polytene band 3C3-3C7), RP98-9H1 (polytene band 15C1-15D6). To
694 make the FISH probes, the BACs were PCR amplified using the Illustra GenomiPhi V2

695 DNA Amplification Kit (GE 25-6600-30). The concentration of the BAC DNA was
696 determined using a Quibit and 10 ng BAC DNA was used per amplification reaction.
697 The amplification reaction was performed via kit protocol. Next, the amplified BAC was
698 restriction enzyme digested using *AluI* (NEB R137S), *HaeII* (NEB R107S), *MseI* (NEB
699 R0525S), *RsaI* (NEB R0167S), *MboI* (NEB R0147S) and *MspI* (NEB R0106S).
700 Following the digestion, the DNA was ethanol precipitated with glycogen
701 (ThermoFisher, 10814010). The precipitated DNA was resuspended in the labeling
702 buffer from the ULYSIS Nucleic Acid Labeling Kits (ThermoFisher – AF647 kit, U21660;
703 AF546 kit, U21652). To label the DNA with AF647 or AF546, the protocol in the ULYSIS
704 Nucleic Acid Labeling Kits was used with 10 µL of the digested BAC DNA. The
705 unreacted dyes were removed from the labeling reaction using Centri-Sep Columns
706 (Princeton Separation, CS-900).
707 FISH with immunohistochemistry was performed as previously described
708 (Christophorou et al., 2013), using anti-mouse C(3)G 1A8-1G2, 5G4-1F1, and 1G5-2F7
709 (all at 1:500) and mouse anti-Orb antibodies 4H8 and 6H4 (1:20 each)(Developmental
710 Studies Hybridoma Bank, Iowa). C(3)G staining was used to identify meiotic nuclei in
711 early, early-mid or mid pachytene with the exception that in *c(3)G*$^{cc\Delta 3}$ mutants mid
712 pachytene oocytes were identified using Orb staining due to the lack of SC present. To
713 measure the 3D distance between the FISH probe foci, a custom ImageJ plug-in ("3D
714 jru v1") was used with a slice spacing of 0.20 and pixel spacing of 0.06370 (available at
715 http://research.stowers.org/imagejplugins). A locus was considered paired if the
716 distance between the FISH probe foci was <0.75 µm and unpaired if the distanced
717 between the FISH probe foci was ≥0.75 µm.

718

719 *Imaging and image analysis*

720 Except for the STED imaging (see below), all images were acquired on an inverted
721 DeltaVision microscopy system (GE Healthcare) with an Olympus 100x Objective
722 (UPlanSApo 100x NA 1.40) and a high-resolution CCD camera or an Applied Precision
723 OMX Blaze microscope (Issaquah, WA, USA) equipped with a PCO Edge sCMOS
724 camera. Images were deconvolved (DeltaVision and OMX) and reconstruction was
725 performed (OMX) using SoftWoRx v. 6.5 software (Applied Precision/GE Healthcare)
726 following Applied Precision protocols. Images were cropped and brightness and
727 contrast was slightly adjusted using ImageJ.

728

729 *Length measurements for the synaptonemal complex*
730
731 These were performed utilizing custom macros in ImageJ (NIH, Bethesda, MD). C(3)G
732 signals corresponding to roughly a single nucleus were traced approximately in 3D as
733 follows. Firstly, structured illumination images were scaled in x and y by 4 with bilinear
734 interpolation. Then they were blurred in x and y with a standard deviation of 8 pixels (80
735 nm). Next a rolling ball background with a radius of 50 pixels was subtracted. The
736 resulting 3D images were thresholded at 25% of their maximum intensity to create a
737 mask encompassing the synaptonemal complex fibers. Objects containing less than
738 500 voxels in 3D corresponded to noise in the image and were removed. Finally, the
739 images were skeletonized in 3D using the 3D skeletonize plugin (based on (Lee et al.,
740 1994), CVGIP: Graphical Models and Image Processing) to create single pixel traces of
741 the SC in three dimensions. These were dilated once to close single pixel gaps and

742 each 3D fiber volume was measured in voxel units for presentation. Single outliers were
743 tested for and removed with the Grubbs test at a 1% confidence level. Statistical
744 assessment of volume differences was accomplished with a two tailed T test.
745
746 *Line Profile Analysis of STED data*
747 Following the profile averaging approach described in (Cahoon et al., 2017) we
748 assessed the width of the SC. Briefly, single slice cross sectional intensity profiles were
749 generated from manually drawn lines across regions of the SC that appeared to be flat
750 in the z dimension (traveled along the selected plane for a substantial distance). We
751 then aligned all of these profiles (as well as the Corolla signals where present) so that
752 the midpoint between the C(3)G C-termini was at 0. Then, the profiles were averaged to
753 create low noise average profile distributions. A standard t-test was used for statistical
754 comparisons between the *c(3)G*$^{cc\Delta 1}$ and wild type, the mean and standard error of the
755 mean (SEM) were reported.
756
757 **Data and software availability**
758 Primary data files for the figures in this paper are publicly accessible
759 at www.stowers.org/research/publications/odr. For data analysis, the custom ImageJ
760 plugins used are available at research.stowers.org/imagejplugins/zipped_plugins.html.
761
762 **Acknowledgements**
763 We thank Claudio Sunkel for antibodies; past and present members of the Hawley lab
764 for helpful discussion and comments on this manuscript; and Angela Miller for editorial

765 and figure preparation assistance. R.S.H. is an American Cancer Society Research
766 Professor.
767

768 ## References

769 Anderson, L.K., Royer, S.M., Page, S.L., McKim, K.S., Lai, A., Lilly, M.A., Hawley, R.S.,
770 2005. Juxtaposition of C(2)M and the transverse filament protein C(3)G within the
771 central region of Drosophila synaptonemal complex. Proc. Natl. Acad. Sci. U. S. A.
772 102, 4482–7. https://doi.org/10.1073/pnas.0500172102
773 Ashburner, M., Golic, K., Hawley, R., 2005. Chromosomes and position effect
774 variegation. In Drosophila: A laboratory handbook, 2nd ed., C. ed. Cold Spring
775 Harbor Laboratory Press, Cold Spring Harbor, NY.
776 Baker, B.S., Hall, J.C., 1976. Meiotic mutants: genic control of meiotic recombination
777 and chromosome segregation. Genet. Biol. Drosoph. Vol. 1a, 351–434.
778 Berchowitz, L., Copenhaver, G., 2010. Genetic Interference: Dont Stand So Close to
779 Me. Curr. Genomics 11, 91–102. https://doi.org/10.2174/138920210790886835
780 Cahoon, C.K., Hawley, R.S., 2016. Regulating the construction and demolition of the
781 synaptonemal complex. Nat. Struct. Mol. Biol. 23, 369–377.
782 https://doi.org/10.1038/nsmb.3208
783 Cahoon, C.K., Yu, Z., Wang, Y., Guo, F., Unruh, J.R., Slaughter, B.D., Hawley, R.S.,
784 2017. Superresolution expansion microscopy reveals the three-dimensional
785 organization of the Drosophila synaptonemal complex. Proc. Natl. Acad. Sci. U. S.
786 A. 114, E6857–E6866. https://doi.org/10.1073/pnas.1705623114
787 Christophorou, N., Rubin, T., Huynh, J.-R., 2013. Synaptonemal Complex Components

788 Promote Centromere Pairing in Pre-meiotic Germ Cells. PLoS Genet. 9, e1004012.
789 https://doi.org/10.1371/journal.pgen.1004012
790 Collins, K.A., Unruh, J.R., Slaughter, B.D., Yu, Z., Lake, C.M., Nielsen, R.J., Box, K.S.,
791 Miller, D.E., Blumenstiel, J.P., Perera, A.G., Malanowski, K.E., Hawley, R.S., 2014.
792 Corolla Is a novel protein that contributes to the architecture of the synaptonemal
793 complex of Drosophila. Genetics 198.
794 Crown, K.N., Miller, D.E., Sekelsky, J., Hawley, R.S., 2018. Local Inversion
795 Heterozygosity Alters Recombination throughout the Genome. Curr. Biol. 28.
796 https://doi.org/10.1016/j.cub.2018.07.004
797 Dernburg, A.F., McDonald, K., Moulder, G., Barstead, R., Dresser, M., Villeneuve, A.M.,
798 1998. Meiotic Recombination in C. elegans Initiates by a Conserved Mechanism
799 and Is Dispensable for Homologous Chromosome Synapsis. Cell 94, 387–398.
800 https://doi.org/10.1016/S0092-8674(00)81481-6
801 Gladstone, M.N., Obeso, D., Chuong, H., Dawson, D.S., 2009. The synaptonemal
802 complex protein Zip1 promotes bi-orientation of centromeres at meiosis I. PLoS
803 Genet. 5, e1000771. https://doi.org/10.1371/journal.pgen.1000771
804 Gong, W.J., McKim, K.S., Hawley, R.S., 2005. All Paired Up with No Place to Go:
805 Pairing, Synapsis, and DSB Formation in a Balancer Heterozygote. PLoS Genet. 1,
806 e67. https://doi.org/10.1371/journal.pgen.0010067
807 Hall, J.C., 1972. CHROMOSOME SEGREGATION INFLUENCED BY TWO ALLELES
808 OF THE MEIOTIC MUTANT c(3)G IN DROSOPHILA MELANOGASTER. Genetics
809 71.
810 Hanlon, S.L., Miller, D.E., Eche, S., Hawley, R.S., 2018. Origin, Composition, and

811 Structure of the Supernumerary B Chromosome of Drosophila melanogaster.
812 Genetics 210, 1197–1212. https://doi.org/10.1534/genetics.118.301478
813 Hassold, T., Hall, H., Hunt, P., 2007. The origin of human aneuploidy: where we have
814 been, where we are going. Hum. Mol. Genet. 16, R203–R208.
815 https://doi.org/10.1093/hmg/ddm243
816 Hawley, R.S., Irick, H., Haddox, D.A., Whitley, M.D., Arbel, T., Jang, J., McKim, K.,
817 Zitron, A.E., New, C., Childs, G., Lohe, A., 1992. There are two mechanisms of
818 achiasmate segregation inDrosophila females, one of which requires
819 heterochromatic homology. Dev. Genet. 13, 440–467.
820 https://doi.org/10.1002/dvg.1020130608
821 Hughes, S.E., Miller, D.E., Miller, A.L., Hawley, R.S., 2018. Female Meiosis: Synapsis,
822 Recombination, and Segregation in Drosophila melanogaster. Genetics 208, 875–
823 908. https://doi.org/10.1534/genetics.117.300081
824 Jaramillo-Lambert, A., Ellefson, M., Villeneuve, A.M., Engebrecht, J., 2007. Differential
825 timing of S phases, X chromosome replication, and meiotic prophase in the C.
826 elegans germ line. Dev. Biol. 308, 206–21.
827 https://doi.org/10.1016/j.ydbio.2007.05.019
828 Jeffress, J.K., Page, S.L., Royer, S.M., Belden, E.D., Blumenstiel, J.P., Anderson, L.K.,
829 Hawley, R.S., 2007. The Formation of the Central Element of the Synaptonemal
830 Complex May Occur by Multiple Mechanisms: The Roles of the N- and C-Terminal
831 Domains of the Drosophila C(3)G Protein in Mediating Synapsis and
832 Recombination. Genetics 177, 2445–2456.
833 https://doi.org/10.1534/genetics.107.078717

834 Jordan, P.W., Karppinen, J., Handel, M.A., 2012. Polo-like kinase is required for
835 synaptonemal complex disassembly and phosphorylation in mouse spermatocytes.
836 J. Cell Sci. 125, 5061–5072. https://doi.org/10.1242/jcs.105015
837 Joyce, E.F., Apostolopoulos, N., Beliveau, B.J., Wu, C. -tin., 2013. Germline Progenitors
838 Escape the Widespread Phenomenon of Homolog Pairing during Drosophila
839 Development. PLoS Genet. 9, e1004013.
840 https://doi.org/10.1371/journal.pgen.1004013
841 Joyce, E.F., McKim, K.S., 2009. Drosophila PCH2 is required for a pachytene
842 checkpoint that monitors double-strand-break-independent events leading to
843 meiotic crossover formation. Genetics 181, 39–51.
844 https://doi.org/10.1534/genetics.108.093112
845 Keeney, S., Giroux, C.N., Kleckner, N., 1997. Meiosis-specific DNA double-strand
846 breaks are catalyzed by Spo11, a member of a widely conserved protein family.
847 Cell 88, 375–84.
848 Krishnan, B., Thomas, S.E., Yan, R., Yamada, H., Zhulin, I.B., McKee, B.D., 2014.
849 *Sisters Unbound* Is Required for Meiotic Centromeric Cohesion in *Drosophila*
850 *melanogaster*. Genetics 198, 947–965.
851 https://doi.org/10.1534/genetics.114.166009
852 Lake, C.M., Holsclaw, J.K., Bellendir, S.P., Sekelsky, J., Hawley, R.S., 2013. The
853 development of a monoclonal antibody recognizing the Drosophila melanogaster
854 phosphorylated histone H2A variant (γ-H2AV). G3 (Bethesda). 3, 1539–43.
855 https://doi.org/10.1534/g3.113.006833
856 Lake, C.M., Nielsen, R.J., Guo, F., Unruh, J.R., Slaughter, B.D., Hawley, R.S., 2015.

857 Vilya, a component of the recombination nodule, is required for meiotic double-
858 strand break formation in Drosophila. Elife 4. https://doi.org/10.7554/eLife.08287
859 Lee, T.C., Kashyap, R.L., Chu, C.N., 1994. Building Skeleton Models via 3-D Medial
860 Surface Axis Thinning Algorithms. CVGIP Graph. Model. Image Process. 56, 462–
861 478. https://doi.org/10.1006/CGIP.1994.1042
862 Libuda, D.E., Uzawa, S., Meyer, B.J., Villeneuve, A.M., 2013. Meiotic chromosome
863 structures constrain and respond to designation of crossover sites. Nature 502,
864 703–6. https://doi.org/10.1038/nature12577
865 Lindsley, D.L., Sandler, L., Counce, S.J., Chandley, A.C., Lewis, K.R., 1977. The
866 Genetic Analysis of Meiosis in Female Drosophila melanogaster [and Discussion].
867 Philos. Trans. R. Soc. B Biol. Sci. 277, 295–312.
868 https://doi.org/10.1098/rstb.1977.0019
869 Lucchesi, J., Ashburner, M., Novitsaki, E., 1976. The genetics and biology of
870 Drosophila.
871 Lupas, A., Dyke, M. Van, Stock, J., 1991. Predicting coiled coils from protein
872 sequences. Science (80-.). 252, 1162–1164.
873 https://doi.org/10.1126/SCIENCE.252.5009.1162
874 Lupas, A.N., Bassler, J., 2017. Coiled Coils - A Model System for the 21st Century.
875 Trends Biochem. Sci. 42, 130–140. https://doi.org/10.1016/j.tibs.2016.10.007
876 Maguire, M.P., 1985. Crossover frequencies within paracentric inversions in maize: the
877 implications for homologue pairing models. Genet. Res. 46, 273–8.
878 Maguire, M.P., Riess, R.W., 1994. The relationship of homologous synapsis and
879 crossing over in a maize inversion. Genetics 137, 281–8.

880 Manheim, E.A., McKim, K.S., 2003. The Synaptonemal complex component C(2)M
881 regulates meiotic crossing over in Drosophila. Curr. Biol. 13, 276–85.
882 McKim, K.S., Hayashi-Hagihara, A., 1998. mei-W68 in Drosophila melanogaster
883 encodes a Spo11 homolog: evidence that the mechanism for initiating meiotic
884 recombination is conserved. Genes Dev. 12, 2932–2942.
885 https://doi.org/10.1101/gad.12.18.2932
886 Mehrotra, S., McKim, K.S., 2006. Temporal Analysis of Meiotic DNA Double-Strand
887 Break Formation and Repair in Drosophila Females. PLoS Genet. 2, e200.
888 https://doi.org/10.1371/journal.pgen.0020200
889 Miller, D.E., Smith, C.B., Kazemi, N.Y., Cockrell, A.J., Arvanitakis, A. V., Blumenstiel,
890 J.P., Jaspersen, S.L., Hawley, R.S., 2016. Whole-Genome Analysis of Individual
891 Meiotic Events in *Drosophila melanogaster* Reveals That Noncrossover Gene
892 Conversions Are Insensitive to Interference and the Centromere Effect. Genetics
893 203, 159–171. https://doi.org/10.1534/genetics.115.186486
894 Miller, D.E., Takeo, S., Nandanan, K., Paulson, A., Gogol, M.M., Noll, A.C., Perera,
895 A.G., Walton, K.N., Gilliland, W.D., Li, H., Staehling, K.K., Blumenstiel, J.P.,
896 Hawley, R.S., 2012. A Whole-Chromosome Analysis of Meiotic Recombination in
897 Drosophila melanogaster. G3 (Bethesda). 2, 249–60.
898 https://doi.org/10.1534/g3.111.001396
899 Mlynarczyk-Evans, S., Villeneuve, A.M., 2017. Time-Course Analysis of Early Meiotic
900 Prophase Events Informs Mechanisms of Homolog Pairing and Synapsis in
901 Caenorhabditis elegans. Genetics 207, 103–114.
902 https://doi.org/10.1534/genetics.117.204172

903 Nadarajan, S., Lambert, T.J., Altendorfer, E., Gao, J., Blower, M.D., Waters, J.C.,
904 Colaiácovo, M.P., 2017. Polo-like kinase-dependent phosphorylation of the
905 synaptonemal complex protein SYP-4 regulates double-strand break formation
906 through a negative feedback loop. Elife 6. https://doi.org/10.7554/eLife.23437
907 Nicklas, R.B., 1974. CHROMOSOME SEGREGATION MECHANISMS. Genetics 78.
908 Page, S., Nielsen, R.J., Teeter, K., Lake, C.M., Ong, S., Wright, K.R., Dean, K.L., Agne,
909 D., Gilliland, W.D., Hawley, R.S., 2007. A germline clone screen for meiotic
910 mutants in Drosophila melanogaster. Fly (Austin). 1, 172–181.
911 https://doi.org/10.4161/fly.4720
912 Page, S.L., Hawley, R.S., 2001. c(3)G encodes a Drosophila synaptonemal complex
913 protein. Genes Dev. 15, 3130–43. https://doi.org/10.1101/gad.935001
914 Page, S.L., Khetani, R.S., Lake, C.M., Nielsen, R.J., Jeffress, J.K., Warren, W.D.,
915 Bickel, S.E., Hawley, R.S., 2008. corona is required for higher-order assembly of
916 transverse filaments into full-length synaptonemal complex in Drosophila oocytes.
917 PLoS Genet. 4, e1000194. https://doi.org/10.1371/journal.pgen.1000194
918 Parry, D.M., Sandler, L., 1974. The genetic identification of a heterochromatic segment
919 on the X chromosome of Drosophila melanogaster. Genetics 77, 535–9.
920 Previato de Almeida, L., Evatt, J.M., Chuong, H.H., Kurdzo, E.L., Eyster, C.A.,
921 Gladstone, M.N., Gómez-H, L., Llano, E., Meyer, R., Pendas, A.M., Pezza, R.J.,
922 Dawson, D.S., 2019. Shugoshin protects centromere pairing and promotes
923 segregation of nonexchange partner chromosomes in meiosis. Proc. Natl. Acad.
924 Sci. 201902526. https://doi.org/10.1073/pnas.1902526116
925 Sato-Carlton, A., Nakamura-Tabuchi, C., Chartrand, S.K., Uchino, T., Carlton, P.M.,

926 2017. Phosphorylation of the synaptonemal complex protein SYP-1 promotes
927 meiotic chromosome segregation. J. Cell Biol. jcb.201707161.
928 https://doi.org/10.1083/jcb.201707161
929 Sherizen, D., Jang, J.K., Bhagat, R., Kato, N., McKim, K.S., 2005. Meiotic
930 recombination in Drosophila females depends on chromosome continuity between
931 genetically defined boundaries. Genetics 169, 767–81.
932 https://doi.org/10.1534/genetics.104.035824
933 Storlazzi, A., Xu, L., Schwacha, A., Kleckner, N., 1996. Synaptonemal complex (SC)
934 component Zip1 plays a role in meiotic recombination independent of SC
935 polymerization along the chromosomes. Proc. Natl. Acad. Sci. U. S. A. 93, 9043–8.
936 Szauter, P., 1984. An analysis of regional constraints on exchange in Drosophila
937 melanogaster using recombination-defective meiotic mutants. Genetics 106, 45–71.
938 Takeo, S., Lake, C.M., Morais-de-Sá, E., Sunkel, C.E., Hawley, R.S., 2011.
939 Synaptonemal complex-dependent centromeric clustering and the initiation of
940 synapsis in Drosophila oocytes. Curr. Biol. 21, 1845–51.
941 https://doi.org/10.1016/j.cub.2011.09.044
942 Tanneti, N.S., Landy, K., Joyce, E.F., McKim, K.S., 2011. A Pathway for Synapsis
943 Initiation during Zygotene in Drosophila Oocytes. Curr. Biol. 21, 1852–1857.
944 https://doi.org/10.1016/j.cub.2011.10.005
945 Tung, K.S., Roeder, G.S., 1998. Meiotic chromosome morphology and behavior in zip1
946 mutants of Saccharomyces cerevisiae. Genetics 149, 817–32.
947 Voelkel-Meiman, K., Cheng, S.-Y., Morehouse, S.J., MacQueen, A.J., 2016.
948 Synaptonemal Complex Proteins of Budding Yeast Define Reciprocal Roles in

949 MutSγ-Mediated Crossover Formation. Genetics 203, 1091–103.
950 https://doi.org/10.1534/genetics.115.182923
951 Wagner, C.R., Kuervers, L., Baillie, D.L., Yanowitz, J.L., 2010. xnd-1 regulates the
952 global recombination landscape in Caenorhabditis elegans. Nature 467, 839–43.
953 https://doi.org/10.1038/nature09429
954 Yan, R., McKee, B.D., 2013. The cohesion protein SOLO associates with SMC1 and is
955 required for synapsis, recombination, homolog bias and cohesion and pairing of
956 centromeres in Drosophila Meiosis. PLoS Genet. 9, e1003637.
957 https://doi.org/10.1371/journal.pgen.1003637
958 Zeng, Y., Li, H., Schweppe, N.M., Hawley, R.S., Gilliland, W.D., 2010. Statistical
959 Analysis of Nondisjunction Assays in Drosophila. Genetics 186, 505–513.
960 https://doi.org/10.1534/genetics.110.118778
961 Zickler, D., Kleckner, N., 2015. Recombination, pairing, and synapsis of homologs
962 during meiosis. Cold Spring Harb. Perspect. Biol. 7, a016626.
963 https://doi.org/10.1101/cshperspect.a016626
964 Zickler, D., Kleckner, N., 1999. Meiotic chromosomes: integrating structure and function.
965 Annu. Rev. Genet. 33, 603–754. https://doi.org/10.1146/annurev.genet.33.1.603
966 Zitron, A.E., Hawley, R.S., 1989. The genetic analysis of distributive segregation in
967 Drosophila melanogaster. I. Isolation and characterization of Aberrant X
968 segregation (Axs), a mutation defective in chromosome partner choice. Genetics
969 122, 801–21.
970
971

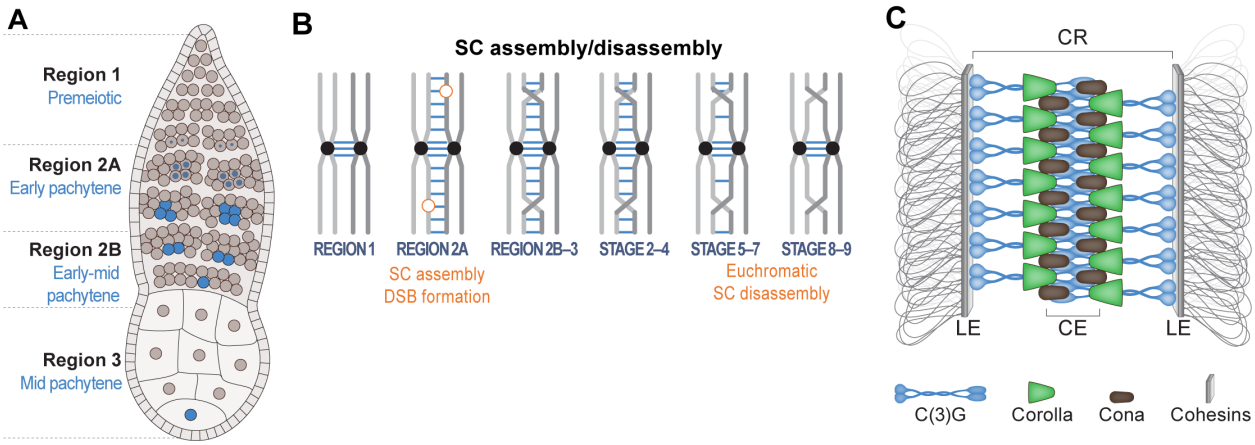

Figure 1: Schematic of early meiosis in *Drosophila*. (A) Diagram of a *Drosophila* germarium and SC formation (described in (Hughes et al., 2018)). At the anterior tip of the germarium, a germline stem cell divides asymmetrically to give rise to a cystoblast, which undergoes four mitotic divisions with incomplete cytokinesis to yield a 16-cell cyst. At region 2A (zygotene/early pachytene) up to 4 of the 16 cells in the cyst will enter meiosis and assemble the SC (SC represented by blue shading) to fully synapse the chromosomes. The oocyte selection process progresses in region 2B and is characterized by two nuclei (pro-oocytes) with full-length SC (early-mid pachytene) and is completed by region 3 (mid pachytene) with only one oocyte per cyst retaining full-length SC and all other nuclei having backed out of the meiotic program to become nurse cells. (B) Homologous chromosome pairing and SC assembly begin at the centromeres (represented as black dots on the chromosomes) during the mitotic divisions in region 1 (Christophorou et al., 2013; Joyce et al., 2013). In region 2A (early pachytene) the SC (represented by blue lines) is assembled along the chromosome arms and DSBs form (orange circles). The SC is maintained along chromosome arms

990 until stage 5-7 (late pachytene), when SC disassembly occurs at multiple regions along
991 the chromosome arms. The SC persists at the centromeres into stages 8–9 (mid
992 prophase)(Takeo et al., 2011; Tanneti et al., 2011). (C) Model of the *Drosophila* SC
993 showing the transverse filament protein C(3)G (blue), the central region (CR) protein
994 Corolla (green), the central element protein CONA (black), and the lateral
995 element/cohesin proteins (grey) connected to chromatin loops (adapted from (Hughes
996 et al., 2018)).
997
998
999

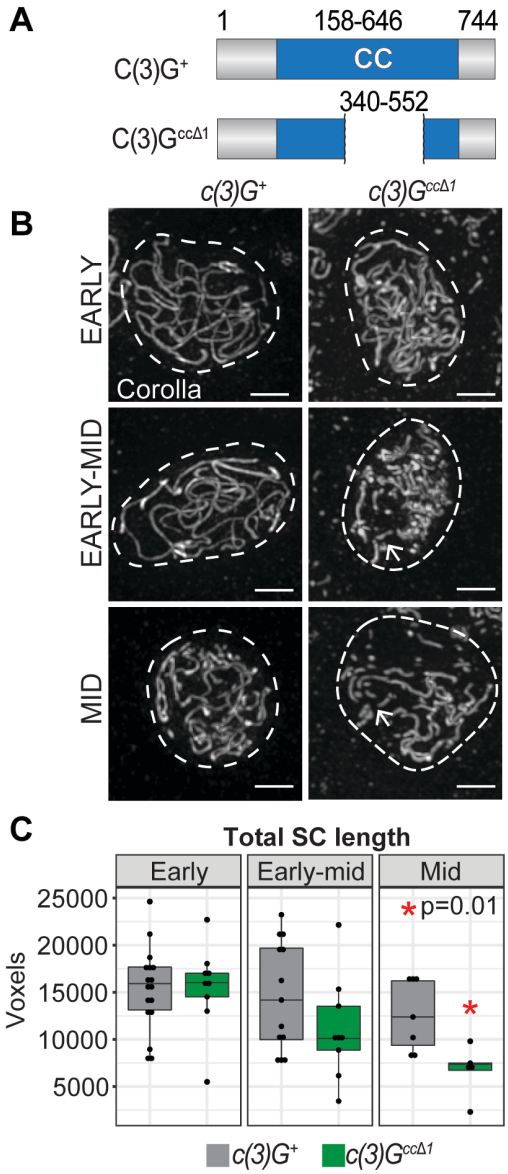

1000

1001 **Figure 2: In-frame deletion of part of the large coiled-coil region of C(3)G leads to**

1002 **a failure to maintain SC.** (A) The *c(3)G*$^{cc\Delta 1}$ deletion removes the amino acids 340–552

1003 from the coiled-coil (CC) domain of C(3)G. The predicted protein CC is in blue (based

1004 on COILs software (Lupas et al., 1991)). (B) Images showing localization of the SC

1005 protein Corolla in *c(3)G*$^{+}$ and *c(3)G*$^{cc\Delta 1}$ nuclei from early pachytene (region 2A) to mid

1006 pachytene (region 3). Dotted lines indicate the location of the nucleus as defined by

1007 DAPI staining (not shown). Arrowheads indicate discontinuities in the SC. Scale bars, 2

1008 μm. (C) Quantification of the total track length of C(3)G-positive SC in nuclei from early,

1009 early-mid and mid pachytene using skeleton analysis (See Methods). *p=0.01 by t-test,

1010 *c(3)G*$^{+}$: N=17 (early), N=13 (early-mid), and N=7 (mid); *c(3)G*$^{cc\Delta 1}$: N=9 (early), N=9

1011 (early-mid), and N=5 (mid).

1012

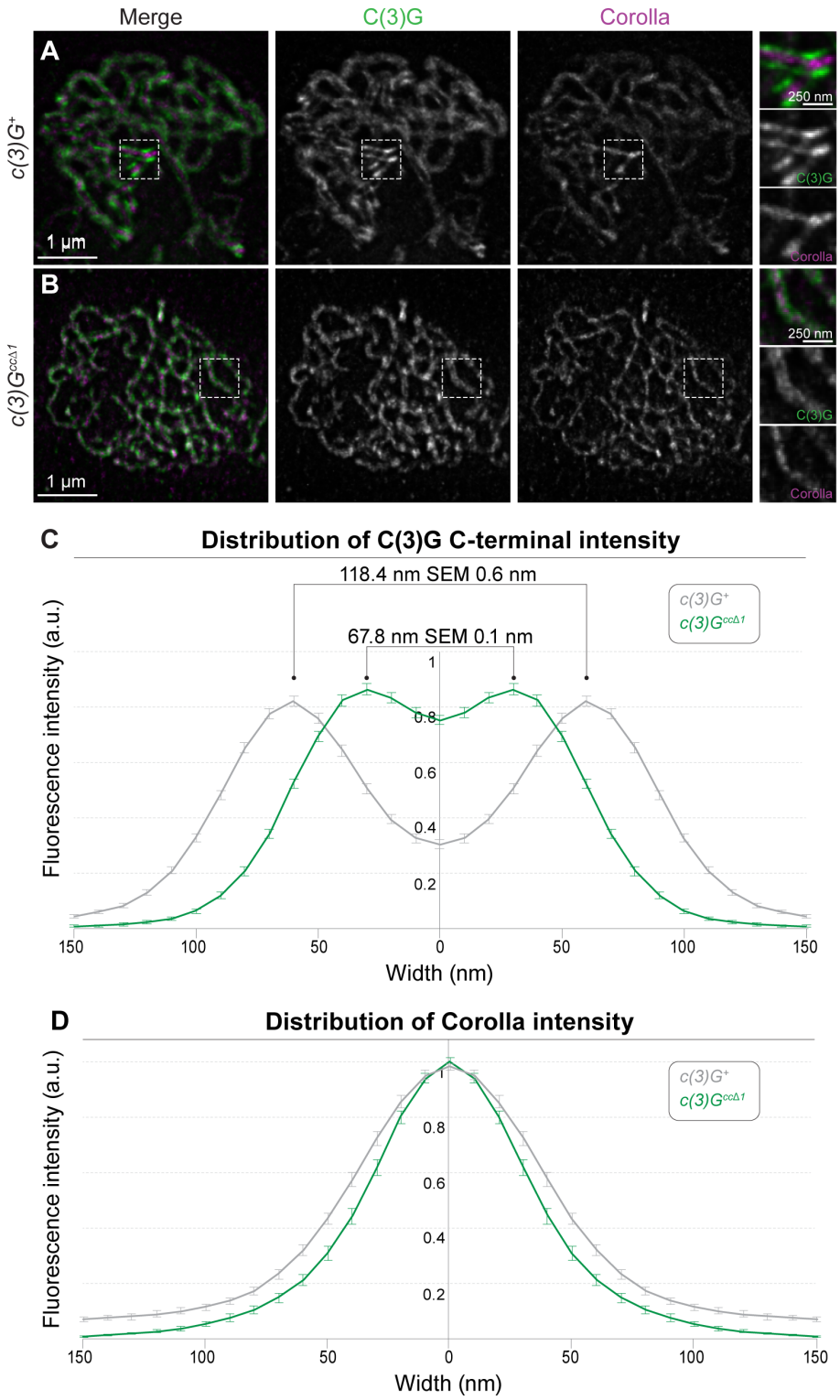

1013

1014 **Figure 2- figure supplement 1: Width of SC is reduced, but the tripartite structure**

1015 **is maintained, in *c(3)G$^{cc\Delta 1}$* mutants in early pachytene.** STED images of early

1016 pachytene nuclei with the C-terminus of C(3)G (green) and Corolla (magenta) labeled in
1017 *c(3)G*$^{+}$ (A) and *c(3)G*$^{cc\Delta 1}$ mutants (B). (C)The average distribution of the distance
1018 between the two C-terminal C(3)G tracks is shown based on a line profile analysis of
1019 STED data in each genotype (see Methods). The quantification resulted in an average
1020 width of 118.4 nm ± 0.6 nm (SEM) in wild type and 67.8 nm ± 0.1 nm (SEM) in *c(3)G*$^{cc\Delta 1}$
1021 mutants. (D) The average distribution of the Corolla signal based on a line profile
1022 analysis of STED data in each genotype. The average distribution was generated by
1023 averaging 46 line profiles from 8 wild type nuclei and 35 line profiles from 12 *c(3)G*$^{cc\Delta 1}$
1024 nuclei.
1025
1026

1027

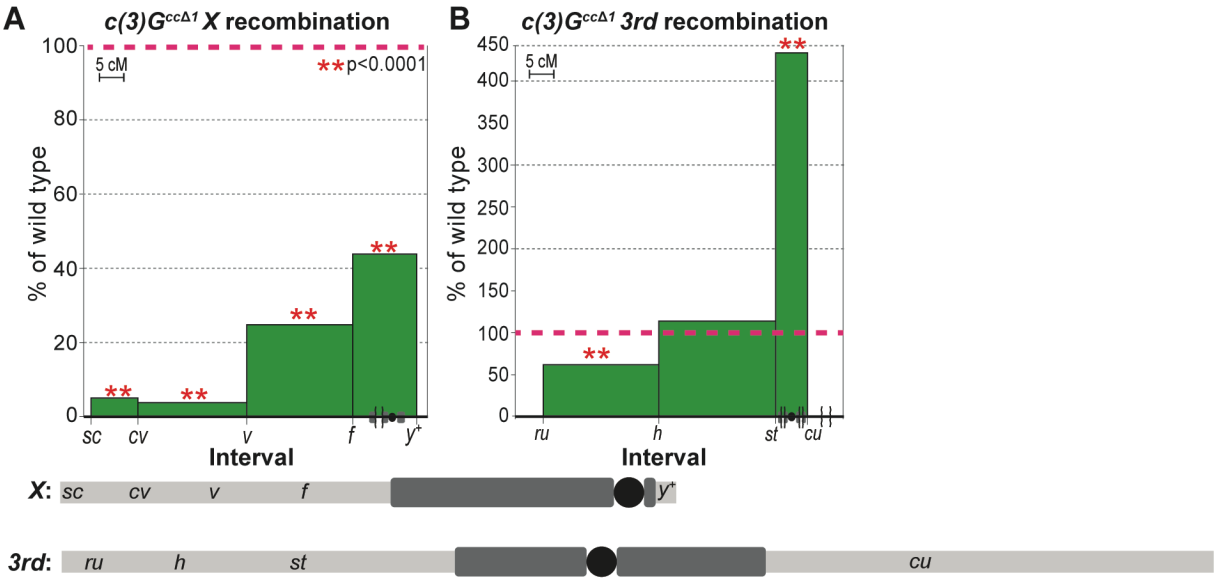

1028

1029 **Figure 3: *c(3)G$^{cc\Delta 1}$* mutants exhibit chromosome-specific defects in**

1030 **recombination.** Recombination in c*(3)G$^{cc\Delta 1}$* females on the *X* chromosome (A) and the

1031 *3rd* chromosome (B) are plotted with percent of wild type on the y-axis vs chromosome

1032 location (in cM) on the x-axis. Brackets along x-axis indicate truncation of that region of

1033 the chromosome. The red dotted line marks wild type levels of recombination and is set

1034 at 100%. P-values obtained using a Fisher's exact test (see Table 1,2 for N values).

1035 See Methods for the recessive markers used to assay recombination. For reference,

1036 below each chart is a diagram of the corresponding chromosome being analyzed

1037 displaying the relative cytological positions of the recombination markers and the

1038 approximate amounts of pericentromeric heterochromatin estimated from (Ashburner et

1039 al., 2005) (the black circle represents the centromere).

1040

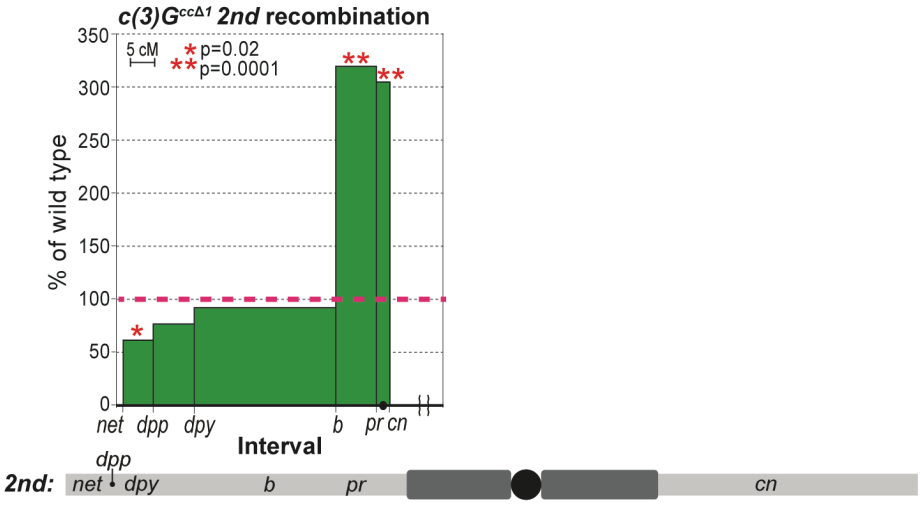

Figure 3- figure supplement 1: *c(3)G*$^{cc\Delta 1}$ mutants exhibit recombination defects on the *2nd* chromosome. Recombination in *c(3)G*$^{cc\Delta 1}$ mutants on the *2nd* chromosome plotted with percent of wild type on the y-axis vs chromosome location (in cM) on the x-axis. Brackets along x-axis indicate truncation of that region of the chromosome. The red dotted line marks wild type levels of recombination and is set to 100%. See Methods for the recessive markers used to assay recombination. P-values obtained using a Fisher's exact test (see Table 3 for N values). For reference, below each chart is a diagram of the corresponding chromosome being analyzed displaying the relative cytological positions of the recombination markers and the approximate amounts of pericentromeric heterochromatin estimated from (Ashburner et al., 2005) (the black circle represents the centromere).

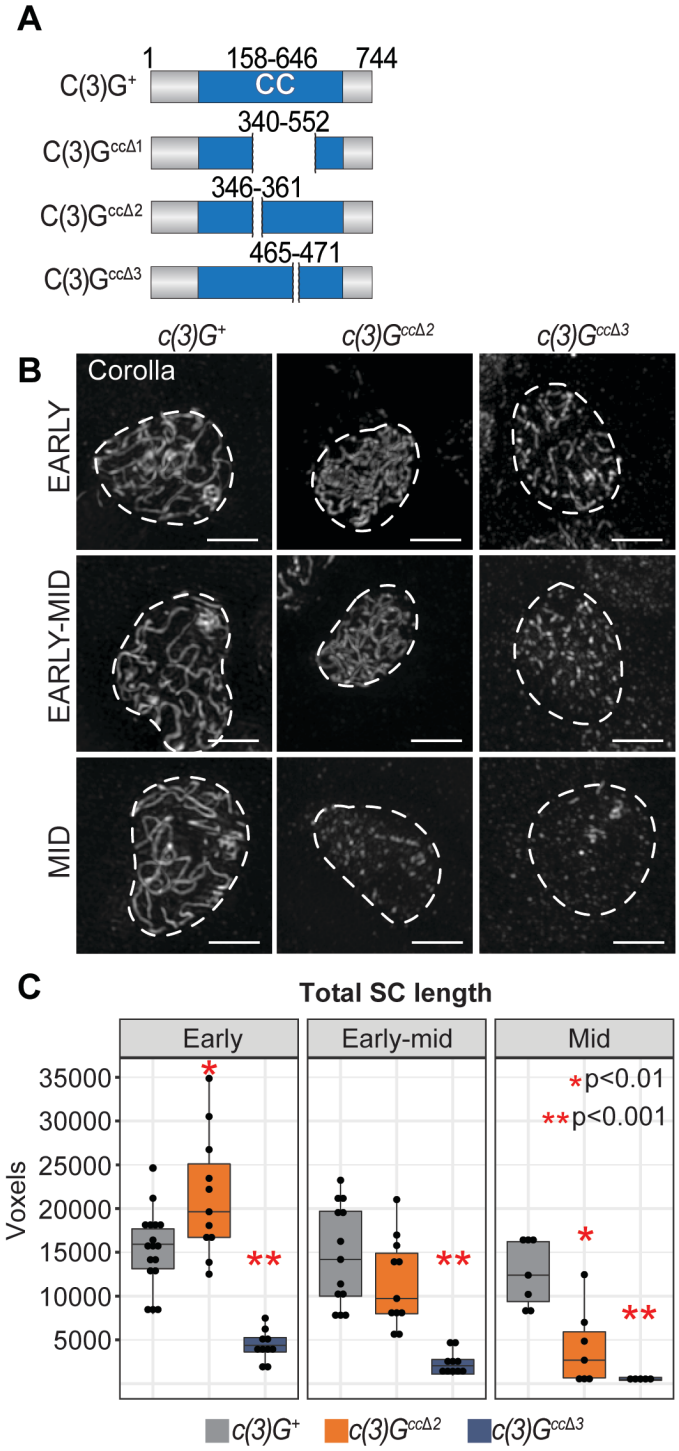

1055

1056 **Figure 4: Two smaller in-frame deletions within the putative *c(3)G* coiled-coil**

1057 **region cause varying levels of SC defects.** (A) Diagrams of the C(3)G^{+}, C(3)G^{ccΔ1},

1058 C(3)G^{ccΔ2} and C(3)G^{ccΔ3} coding regions. (B) Images showing localization of the SC

1059 protein Corolla in *c(3)G*$^{+}$, *c(3)G*$^{cc\Delta 2}$, and *c(3)G*$^{cc\Delta 3}$ mutants from early pachytene (region
1060 2A) to mid pachytene (region 3). Dotted lines indicate the location of the nucleus as
1061 defined by DAPI staining (not shown). Scale bars, 2 μm. (C) Quantification of the total
1062 length of C(3)G positive SC in nuclei from early, early-mid and mid pachytene using
1063 skeleton analysis (See Methods). *c(3)G*$^{+}$ controls are the same ones used in Fig 2.
1064 *p<.01 and **p<.001 by t-test. *c(3)G*$^{cc\Delta 2}$: N=11 (early), N=11 (early-mid), and N=7 (mid);
1065 *c(3)G*$^{cc\Delta 3}$: N=10 (early), N=10 (early-mid), and N=5 (mid).
1066

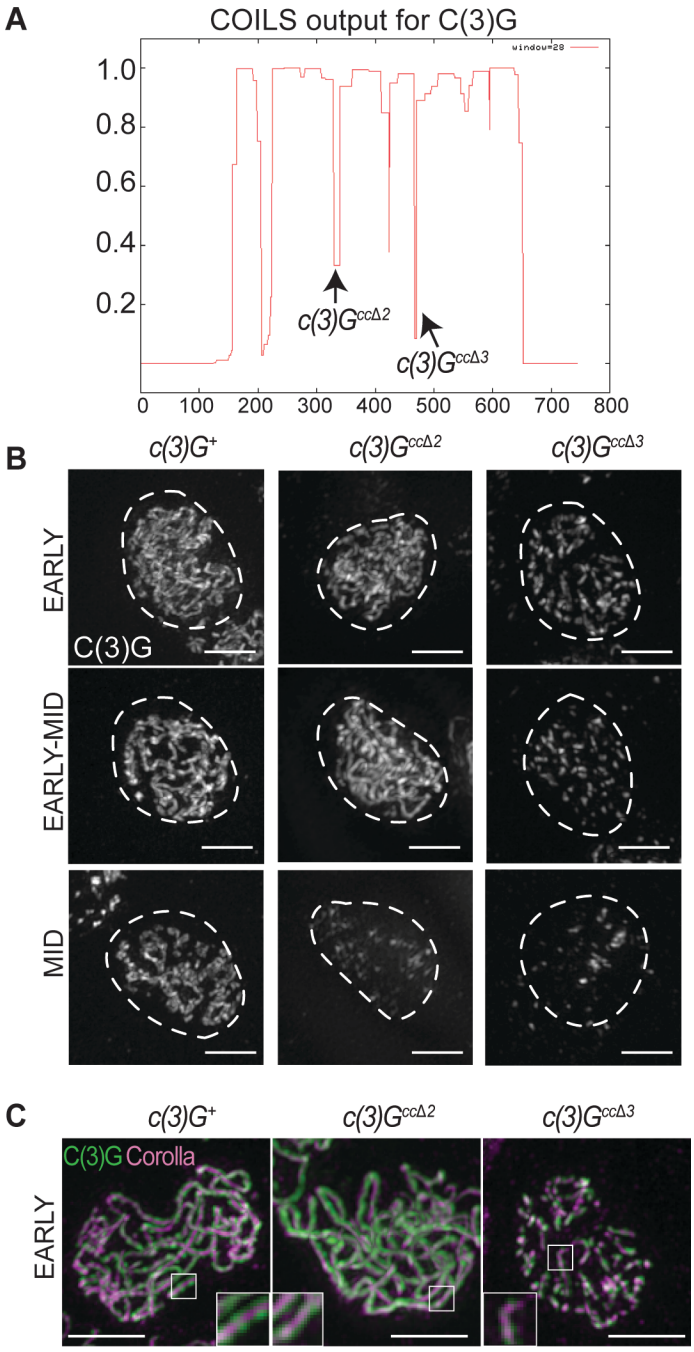

1067

1068 **Figure 4- figure supplement 1: C(3)G is present in *c(3)G^{ccΔ2}* and *c(3)G^{ccΔ3}* mutants.**

1069 (A) Diagram of COILS score along the length of C(3)G with arrows where *c(3)G^{ccΔ2}* and

1070 *c(3)G^{ccΔ3}* deletions were made (Lupas et al., 1991). (B) Images showing localization of

1071 the SC protein C(3)G in wild type, *c(3)G^{ccΔ2}*, and *c(3)G^{ccΔ3}* flies from early pachytene

1072 (region 2A) to mid pachytene (region 3). Dotted lines indicate the location of the nucleus

1073 as defined by DAPI staining (not shown). (C) Combined Corolla (magenta) and C(3)G

1074 (green) staining in early pachytene nuclei show localization of Corolla to the middle of

1075 C(3)G. Scale bars, 2 μm.

1076

1077

1078

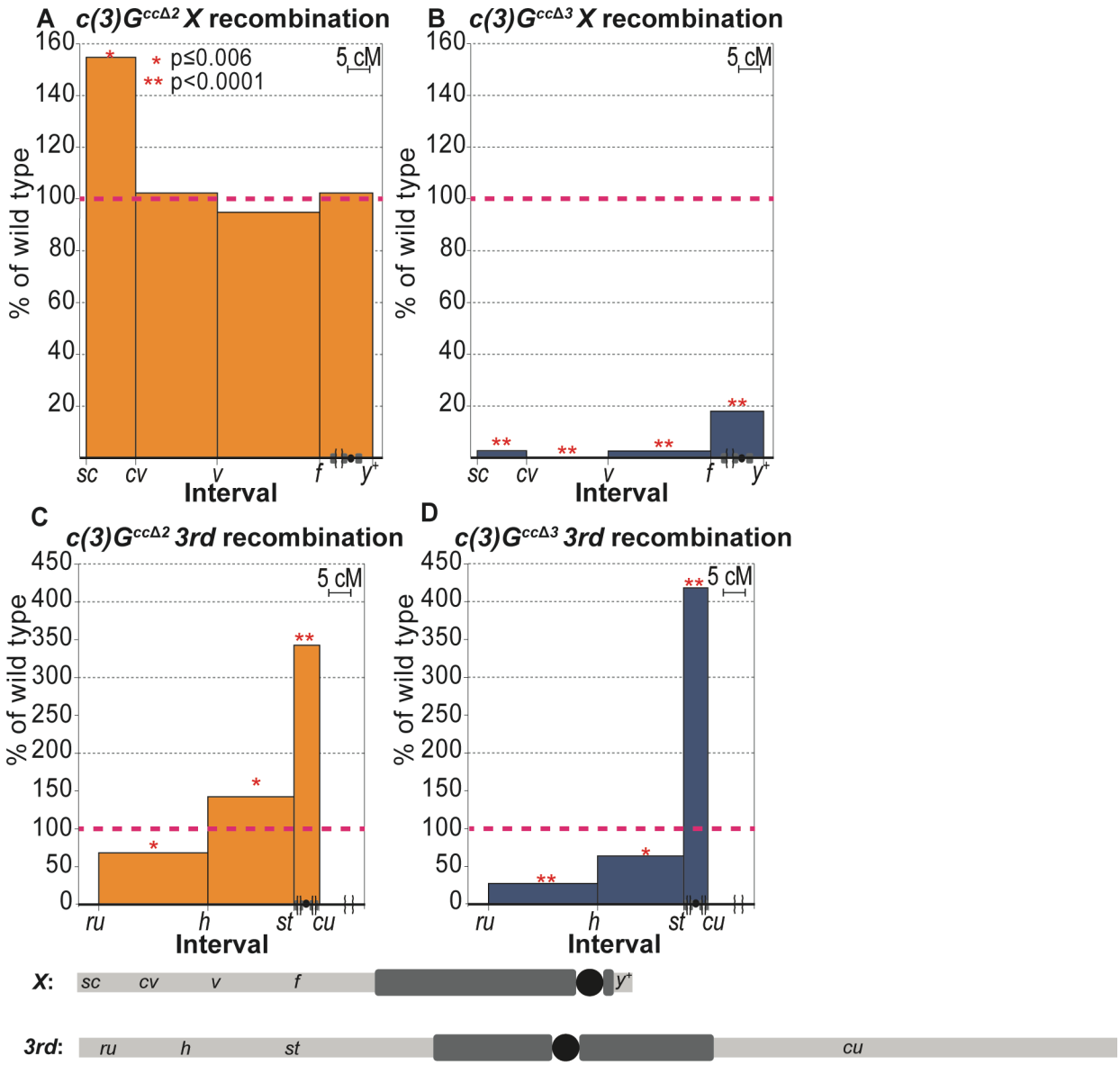

1079

1080 **Figure 5: Loss of SC maintenance in *c(3)G*$^{cc\Delta 2}$ mutants in mid pachytene is not**

1081 **sufficient to disrupt *X* chromosome recombination.** Recombination in c*(3)G*$^{cc\Delta 2}$ and

1082 c*(3)G*$^{cc\Delta 3}$ females on the *X* chromosome (A,B) and the *3rd* chromosome (C,D) are

1083 plotted with percent of wild type on the y-axis vs chromosome location (in cM) on the x-

1084 axis. Brackets along x-axis indicate truncation of that region of the chromosome. The

1085 red dotted line marks wild type levels of recombination and is set at 100%. P-values

1086 obtained using a Fisher's exact test (see Table 1,2 for N values). See Methods for the
1087 recessive markers used to assay recombination. For reference, below each chart is a
1088 diagram of the corresponding chromosome being analyzed displaying the relative
1089 cytological positions of the recombination markers and the approximate amounts of
1090 pericentromeric heterochromatin estimated from (Ashburner et al., 2005) (the black
1091 circle represents the centromere).
1092
1093
1094
1095
1096

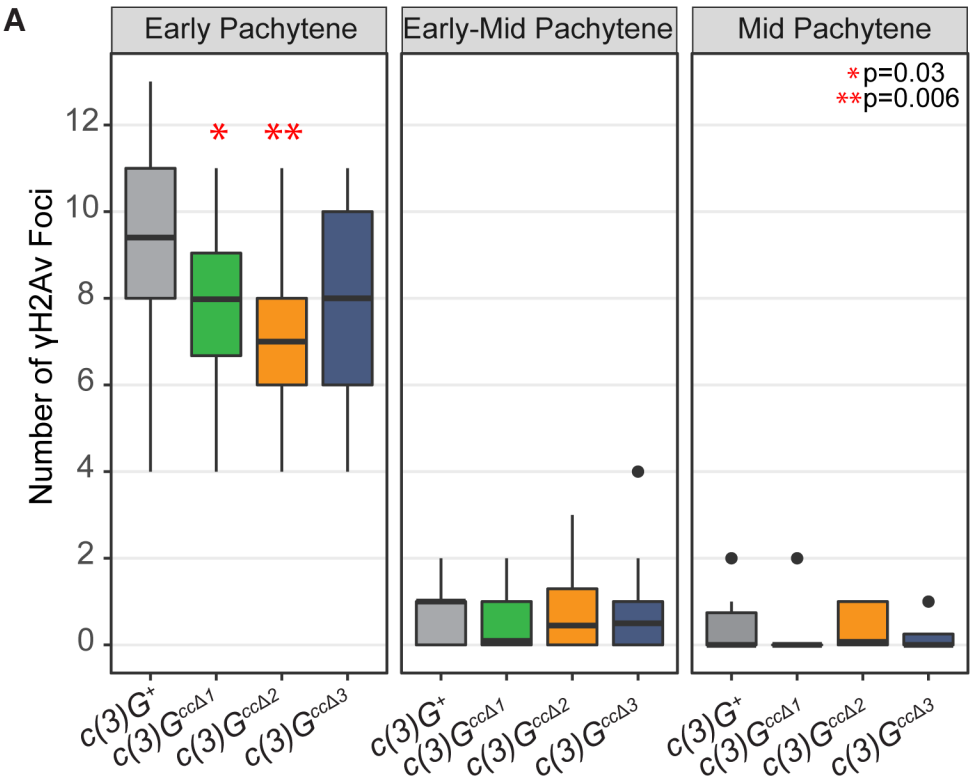

B

3rd chromosome recombination frequency

Genotype	*ru-h*	*h-st*	*st-cu*	total	N
c(3)G^{+}	23.0	21.7	6.1	50.9	525
c(3)G$^{cc\Delta 3}$	6.3	11.7	27.5	45.5	615
vilya^{826}*; +; c(3)G*$^{cc\Delta 3}$	0.5	0.0	0.9	1.4	214

Figure 5- figure supplement 1: DSB levels, as determined by γH2AV foci number, in *c(3)G*$^{cc\Delta 1}$, *c(3)G*$^{cc\Delta 2}$ and *c(3)G*$^{cc\Delta 3}$ mutants are similar to wild type.

(A) Quantification of the number of DSBs per nucleus was determined by counting the number of γH2AV foci in early, early-mid and mid pachytene of the germarium for *c(3)G*$^{+}$, *c(3)G*$^{cc\Delta 1}$, *c(3)G*$^{cc\Delta 2}$ and *c(3)G*$^{cc\Delta 3}$ flies. N value is ≥ 10 nuclei. Statistics were performed using the Mann-Whitney test. (B) *3rd* chromosome recombination frequency in *c(3)G*$^{+}$, *c(3)G*$^{cc\Delta 3}$ and, *vilya*^{826}*;c(3)G*$^{cc\Delta 3}$ double mutants. Data for *c(3)G*$^{cc\Delta 3}$ is the same as shown in Figure 5 and Table 2.

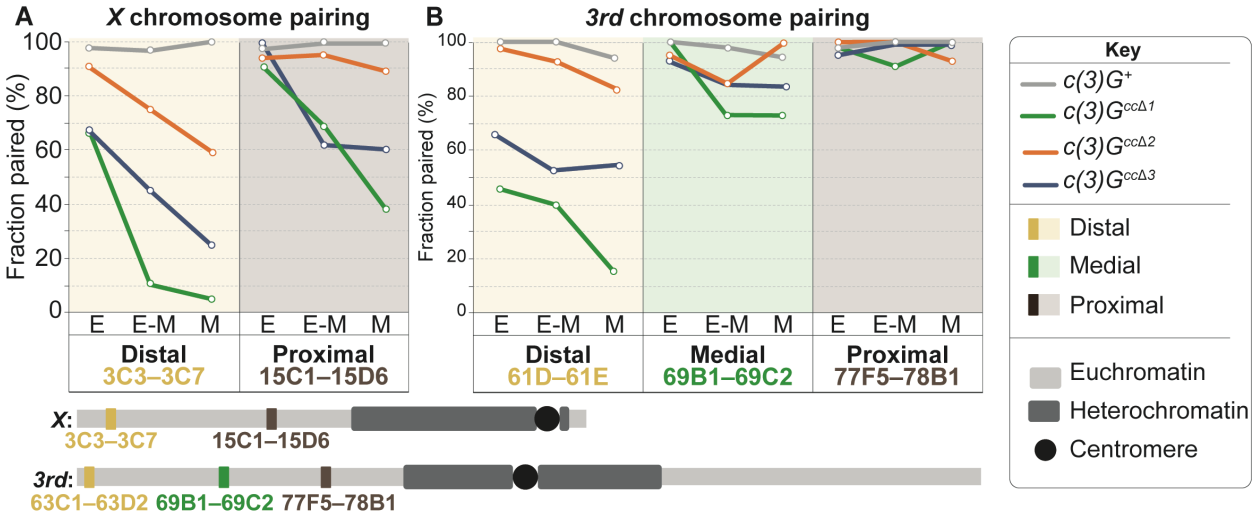

Figure 6: SC in early to mid pachytene maintains homologous chromosome pairing. Fraction of paired euchromatic regions in *c(3)G*$^{+}$ controls (grey line), *c(3)G*$^{cc\Delta 1}$ (green line), *c(3)G*$^{cc\Delta 2}$ (orange line), and *c(3)G*$^{cc\Delta 3}$ flies (blue line) assessed by FISH using BAC probes against either centromere-distal or -proximal regions on the *X* chromosome (A) and centromere-distal, -medial or -proximal regions on the *3rd* chromosome (B) at early (E), early-mid (E-M) or mid (M) pachytene. For reference, below each chart is a diagram of the corresponding chromosome being analyzed (the black circle represents the centromere). For N-values see Table 5.

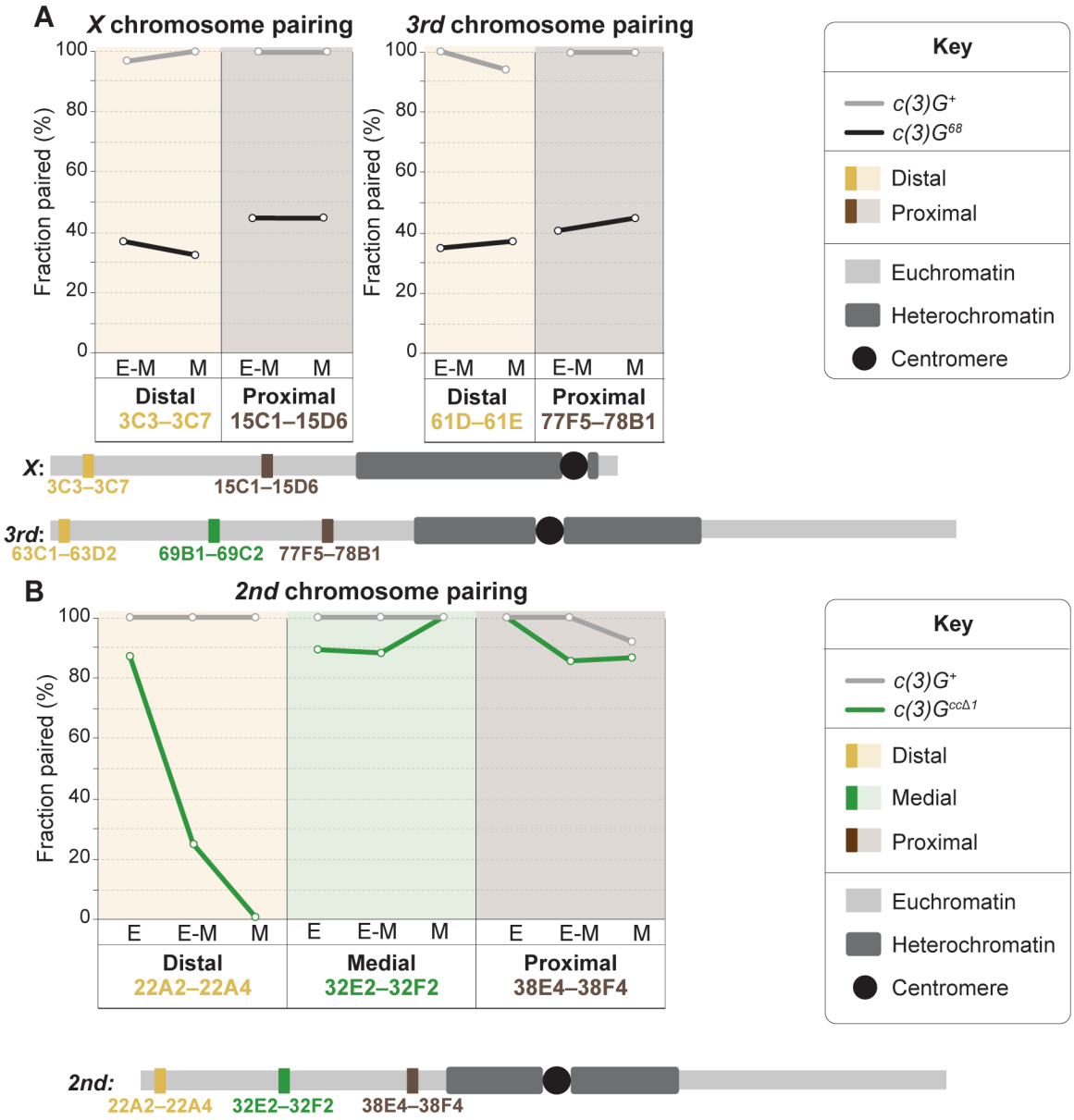

Figure 6- figure supplement 1: Pairing in *c(3)G*^{68} and *c(3)G*^{ccΔ1} mutants

(A) Fraction of paired euchromatic regions assessed by FISH using BAC probes against centromere-distal and proximal regions of the *X* and *3rd* chromosomes in *c(3)G*^{68} (black line) mutants at early-mid (E-M) or mid (M) pachytene. *c(3)G*$^{+}$ control data was previously presented in Figure 6. (B) Fraction of paired euchromatic regions on the *2nd*

1126 chromosome at early (E), early-mid (E-M) or mid (M) pachytene in *c(3)G*$^{cc\Delta 1}$ (green line)

1127 mutants compared to *c(3)G*$^{+}$ (grey line) controls. See Table 5 for N values.

1128

1129

1130

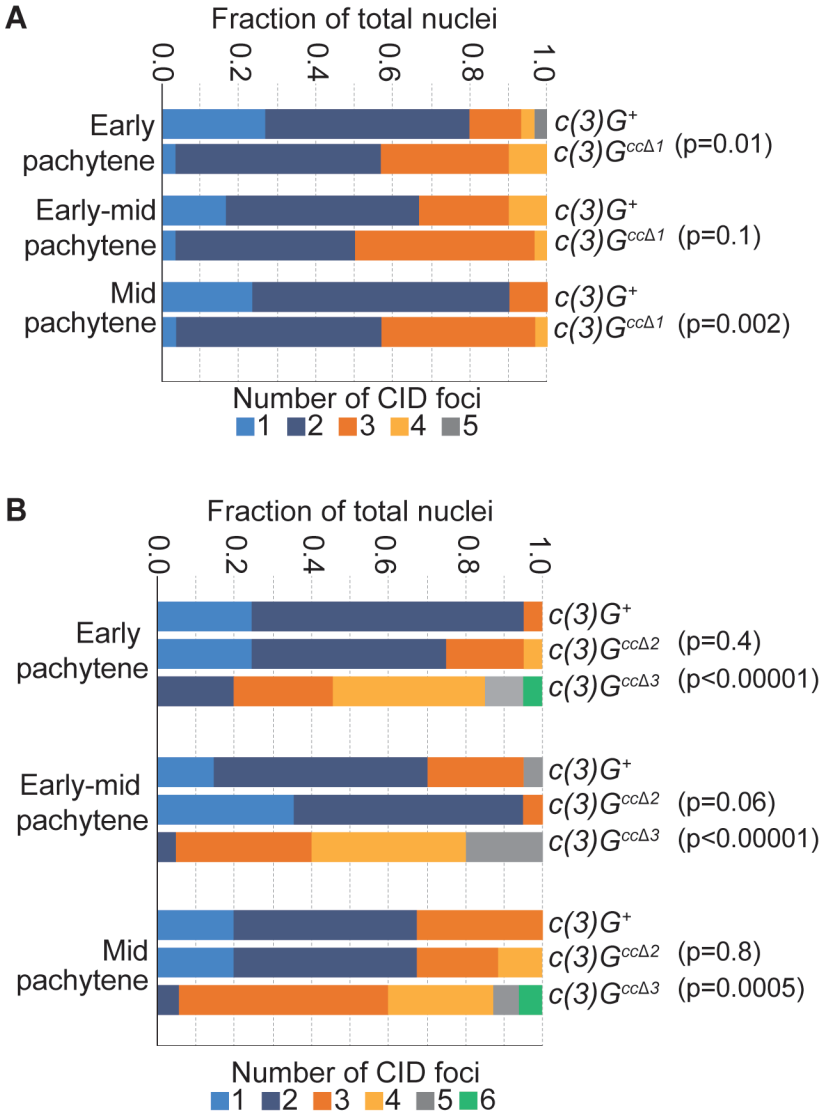

1131

1132 **Figure 6- figure supplement 2: Centromere pairing *c(3)G*$^{cc\Delta 1}$, *c(3)G*$^{cc\Delta 2}$, and**

1133 ***c(3)G*$^{cc\Delta 3}$ mutants**

1134 Quantification of the number of CID foci per nucleus in wild type, *c(3)G*$^{cc\Delta 1}$(A), *c(3)G*$^{cc\Delta 2}$

1135 (B), and *c(3)G*$^{cc\Delta 3}$ mutants (B) from early pachytene (region 2A) to mid pachytene

1136 (region 3) shows no loss of centromere pairing. Statistics were performed using the

1137 Mann-Whitney test. N ≥ 15.

1138

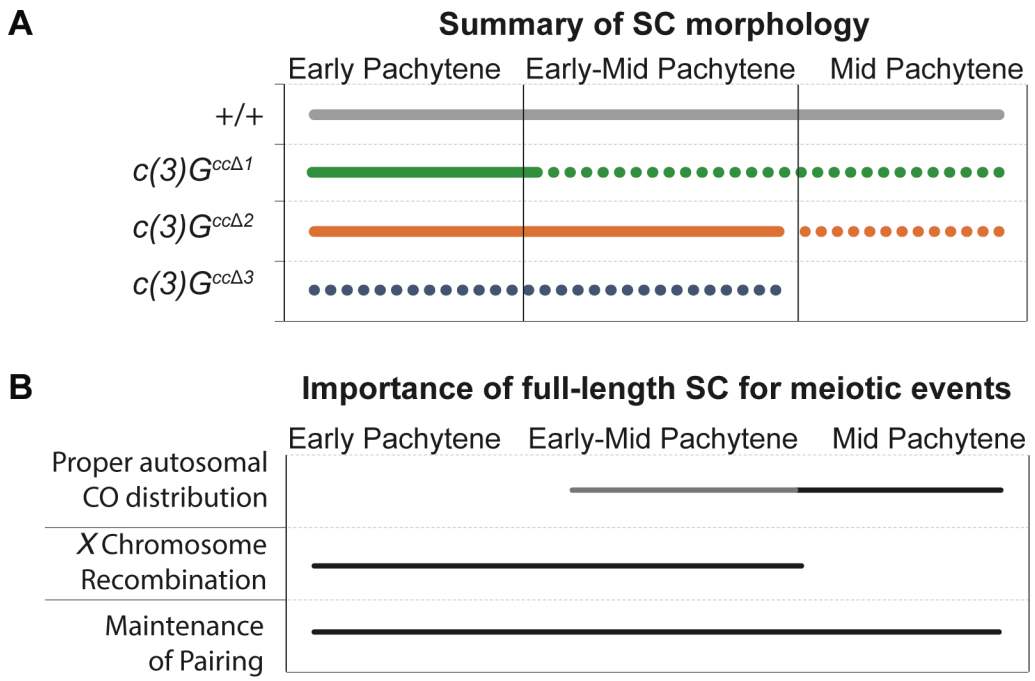

1139

1140 **Figure 7: Summary of SC morphology and model of the requirement for SC in**

1141 **recombination and pairing maintenance.**

1142 (A) Summary of SC phenotypes in *c(3)G*$^{+}$ (grey line), *c(3)G*^{ccΔ1} (green line), *c(3)G*^{ccΔ2}

1143 (orange line) and *c(3)G*^{ccΔ3} (blue line) flies. *c(3)G*^{ccΔ1} flies displayed SC defects in early-

1144 mid pachytene while *c(3)G*^{ccΔ2} flies lost SC in mid pachytene. *c(3)G*^{ccΔ3} flies never fully

1145 assembled SC. Dotted line indicates defects in total SC length and fragmentation (B) A

1146 model of the requirement of full-length SC (black lines) at different stages of pachytene.

1147 Based on our data we propose that full-length SC is important for proper autosomal

1148 crossover placement, *X* chromosome recombination and maintenance of pairing at

1149 different stages of early to mid pachytene. The grey line represents a potential role for

1150 full-length SC that cannot be confirmed with our data.

1151

1152

Table 1. *X* Chromosome Recombination

Maternal genotype	*c(3)G*$^{+}$	*c(3)G*$^{cc\Delta 1}$	*c(3)G*$^{+}$	*c(3)G*$^{cc\Delta 2}$	*c(3)G*$^{cc\Delta 3}$
	(N=1515)	(N=1420)	(N = 1721)	(N = 1119)	(N = 401)
Map Length (% compared to *c(3)G*$^{+}$)					
sc–cv	8.8	0.4 (4.5%)	10.6	16.6 (157%)	0.3 (2.8%)
cv–v	20.7	0.7 (3.4%)	18.1	18.5 (102%)	0.0 (0.0%)
v–f	21.1	5.2 (24.6%)	21.8	20.7 (95%)	0.5 (2.3%)
f–y^{+}	12.4	5.4 (43.5%)	11.2	11.5 (102%)	2.0 (17.9%)
Total	**63.0**	**11.8 (18.7%)**	**61.7**	**67.4 (109%)**	**2.8 (4.5%)**
Interference					
sc/cv/v	0.7	n/a*	0.5	0.8	n/a*
cv/v/f	0.6	n/a*	0.4	0.5	n/a*
Class					
NCO	688	1264	812	475	390
SCO	703	147	764	537	11
DCO	120	7	137	104	0
TCO	4	2	8	3	0
Exchange rank					
E_0	0.067	0.790	0.103	0.034	0.945
E_1	0.627	0.196	0.597	0.604	0.054
E_2	0.285	0.003	0.263	0.339	0
E_3	0.021	0.011	0.037	0.021	0

1153 Abbreviations: N, total number of flies scored; NCO, chromatids recovered exhibiting no crossovers;
1154 SCO, single-crossover chromatids; DCO, double-crossover chromatids; TCO, triple-crossover
1155 chromatids. *Interference was not calculated unless there were at least 10 DCOs and was not
1156 calculated across the centromere. *c(3)G*$^{+}$ is *y w; pol.*
1157
1158
1159
1160
1161
1162
1163
1164
1165
1166
1167
1168
1169
1170
1171
1172
1173
1174
1175
1176
1177

1178
1179

Table 2. 3rd Chromosome Recombination

Maternal genotype	*c(3)G*$^{+}$	*c(3)G*$^{cc\Delta 1}$	*c(3)G*$^{+}$	*c(3)G*$^{cc\Delta 2}$	*c(3)G*$^{cc\Delta 3}$
	(N=1014)	(N=1385)	(N = 1994)	(N = 931)	(N = 615)
Map Length (% compared to *c(3)G*$^{+}$)					
ru–h	22.5	13.1 (58.2%)	24.7	16.2 (65.5%)	6.3 (25.5%)
h–st	22.4	24.0 (107%)	18.9	26.6 (141%)	11.7 (61.9%)
st–cu	6.1	27.3 (447%)	6.8	23.6 (347%)	27.5 (404%)
Total	**50.9**	**64.4 (126%)**	**50.4**	**66.4 (141%)**	**45.5 (90.3%)**
Interference					
ru/h/st	0.7	0.5	0.8	0.6	n/a*
Class					
NCO	546	675	1069	418	377
SCO	421	535	842	411	199
DCO	45	167	83	99	36
TCO	2	8	0	3	3
Exchange rank					
E_0	0.165	0.202	0.155	0.111	0.343
E_1	0.665	0.420	0.678	0.477	0.442
E_2	0.154	0.345	0.166	0.387	0.176
E_3	0.016	0.032	0.000	0.026	0.039

1180 Abbreviations: N, total number of flies scored; NCO, chromatids recovered exhibiting no
1181 crossovers; SCO, single-crossover chromatids; DCO, double-crossover chromatids; TCO, triple-
1182 crossover chromatids. *Interference was not calculated unless there were at least 10 DCOs in
1183 those intervals and was not calculated across the centromere. *c(3)G*$^{+}$ is *y w; pol.*
1184
1185
1186
1187

Table 3. 2nd Chromosome Recombination		
Maternal genotype	*c(3)G*$^{+}$	*c(3)G*$^{cc\Delta 1}$
	(N = 2376)	(N = 1456)
Map Length (% compared to *c(3)G*$^{+}$)		
net–dpp	5.7	3.4 (59.6%)
dpp–dpy	8.0	5.8 (72.5%)
dpy–b	28.5	26.9 (94.4%)
b–pr	7.8	24.9 (319%)
pr–cn	2.2	6.7 (304%)
Total	**52.2**	**67.6 (129%)**
net/dpp/dpy	0.3	0.8
dpp/dpy/b	0.6	0.8
dpy/b/pr	0.6	-0.2
NCO	1249	624
SCO	1021	692
DCO	98	128
TCO	8	12
E_0	0.134	0.033
E_1	0.715	0.648
E_2	0.125	0.253
E_3	0.027	0.066

Abbreviations: N, total number of flies scored; NCO, chromatids recovered exhibiting no crossovers; SCO, single-crossover chromatids; DCO, double-crossover chromatids; TCO, triple-crossover chromatids. *Interference was not calculated unless there were at least 10 DCOs and was not calculated across the centromere. *c(3)G*$^{+}$ is *y w; pol.*

1216
1217

Table 4. *X* and *4th* Chromosome Nondisjunction					
Maternal genotype	*c(3)G*$^{+}$	*c(3)G*$^{cc\Delta 1}$	*c(3)G*$^{+}$	*c(3)G*$^{cc\Delta 2}$	*c(3)G*$^{cc\Delta 3}$
	(N=1348)	(N=954)	(N = 1157)	(N = 2422)	(N = 837)
Percent nondisjunction (p value)					
X	0.7	1.5	1.0	0.5	4.5*
4th	0.4	0.6	0.1	0.1	2.0*

1218
1219 Rate of *X* and *4th* nondisjunction in *c(3)G*$^{+}$, *c(3)*G$^{cc\Delta 1}$, c*(3)G*$^{cc\Delta 2}$, and *c(3)G*$^{cc\Delta 3}$ females.
1220 Significance calculated as described in (Zeng et al., 2010). Adjusted n accounts for the
1221 inviable progeny class plus the scored progeny. **c(3)G*$^{cc\Delta 3}$ females display elevated rates of
1222 both *X* ($p < .001$) and *4th* ($p<.001$) nondisjunction when compared to *c(3)G*$^{+}$ controls;
1223 however the number of flies scored is not sufficient to determine significance.
1224
1225

Table 5. Summary of *X* and *3rd* chromosome pairing

Maternal genotype	*c(3)G*$^{+}$	*c(3)G*$^{cc\Delta 1}$	*c(3)G*$^{cc\Delta 2}$	*c(3)G*$^{cc\Delta 3}$	*c(3)G*^{68}
Percent paired (N value)					
X proximal (3C3-3C7)					
Early	97.1(70)	67.9(28)	90.9(33)	68.8(16)	n/a
Early-mid	96.6(60)	10.7(28)	75(20)	45(20)	37(27)
Mid	100(24)	5.3(19)	58.8(17)	26.3(19)	36.8(19)
X distal (15C1-15D6)					
Early	97.4(79)	90.6(32)	93.9(33)	100(17)	n/a
Early-mid	100(69)	69(29)	95(20)	62.5(16)	50(18)
Mid	100(28)	38.5(13)	88.2(17)	60(15)	53(15)
2nd proximal (22A2-22A4)					
Early	100(21)	87.5(24)	n/a	n/a	n/a
Early-mid	100(20)	25(20)	n/a	n/a	n/a
Mid	100(13)	1(9)	n/a	n/a	n/a
2nd medial (32E2-32F2)					
Early	100(21)	89.7(29)	n/a	n/a	n/a
Early-mid	100(15)	88.2(17)	n/a	n/a	n/a
Mid	100(8)	100(7)	n/a	n/a	n/a
2nd distal (38E4-38F4)					
Early	100(25)	100(37)	n/a	n/a	n/a
Early-mid	100(23)	85.7(28)	n/a	n/a	n/a
Mid	92.3(13)	86.7(15)	n/a	n/a	n/a
3rd proximal (61D-61E)					
Early	100(36)	45.8(24)	97.6(41)	68.4(19)	n/a
Early-mid	100(32)	40(20)	92.9(28)	52.6(19)	29.2(24)
Mid	93.8(16)	15.4(13)	83.3(24)	56.3(16)	40(15)
3rd medial (69B1-69C2)					
Early	100(46)	100(33)	95.5(22)	93.3(30)	n/a
Early-mid	97.6(43)	73.1(26)	85.7(14)	86.7(15)	n/a
Mid	94.4(18)	73.6(19)	100(9)	84(25)	n/a
3rd distal (77F5-78B1)					
Early	98.2(56)	98.1(54)	100(21)	96(25)	n/a
Early-mid	100(50)	90.9(33)	100(15)	100(17)	41.6(24)
Mid	100(20)	100(17)	93.8(16)	100(18)	50(16)

1226

1227

1228

1229

1230

1231

1232

1233 **Key Resource Table**

RESOURCE/ REAGENT	SOURCE	IDENTIFIER
Antibodies		
C(3)G mouse C-terminal monoclonals	Hawley Lab	1A8-1G2 5G4-1F1 1G5-2F7
Corolla rabbit	Hawley Lab	AP-Corolla
CID rat	Gift from Claudio Sunkel	
CID rat	Hawley Lab	
γH2AV mouse	Iowa Hybridoma Bank	UNC93-5.2.1
Alexa Fluor 488 goat anti-mouse	ThermoFisher	A11001
Alexa Fluor 555 goat anti-mouse	ThermoFisher	A21422
Alexa Fluor 647 goat anti-mouse	ThermoFisher	A21235
Alexa Fluor 488 goat anti-rabbit	ThermoFisher	A11008
Alexa Fluor 555 goat anti-rabbit	ThermoFisher	A21428
Alexa Fluor 555 goat anti-rat	ThermoFisher	A21434
Alexa Fluor 647 goat anti-rat	ThermoFisher	A21247
Bacterial Strains		
TOP10 chemically competent cells	ThermoFisher	C404003
Drosophila BAC RP98-28O9 (polytene band 22A2-22A4)	Children's Hospital Oakland Research Institute (CHORI)	RP98-28O9
Drosophila BAC RP98-43K24 (polytene band 32E2-32F2)	CHORI	RP98-43K24
Drosophila BAC RP98-7D17 (polytene band 38E4-38F4)	CHORI	RP98-7D17
Drosophila BAC RP98-2N23 (polytene band 61D-61E)	CHORI	RP98-2N23
Drosophila BAC RP98-26C20 (polytene band 69B1-69C2)	CHORI	RP98-26C20
Drosophila BAC RP98-3J2 (polytene band 77F5-78B1)	CHORI	RP98-3J2
Drosophila BAC RP98-3D13 (polytene band 3C3-3C7)	CHORI	RP98-3D13
Drosophila BAC RP98-9H1 (polytene band 15C1-15D6)	CHORI	RP98-9H1
Chemicals and Reagents		
AarI restriction enzyme	ThermoFisher	ER1581
SapI restriction enzyme (also known as LguI)	ThermoFisher	ER1931
Antarctic phosphatase	New England Biolabs	M0289S
T4 DNA ligase	New England Biolabs	M0202S
BbsI restriction enzyme	New England Biolabs	R0539S

AluI restriction enzyme	New England Biolabs	R0137S
HaeII restriction enzyme	New England Biolabs	R0107S
MseI restriction enzyme	New England Biolabs	R0525S
RsaI restriction enzyme	New England Biolabs	R0167S
SpeI restriction enzyme	New England Biolabs	R0133S
NdeI restriction enzyme	New England Biolabs	R0111S
MboI restriction enzyme	New England Biolabs	R0147S
MspI restriction enzyme	New England Biolabs	R0106S
Nonidet-P40	Sigma-Aldrich	11332473001
16% Formaldehyde	Electron Microscopy Sciences	15710
Prolong Gold	Life Technologies	P36930
2,2-thiodiethanol (TDE)	VWR	700008-210
VECTASHIELD	VWR	101098-042
Glycogen	ThermoFisher	10814010
Critical Commercial Assays		
Quik Change II XL Site-Directed Mutagenesis Kit	Stratagene/Agilent Technologies	200521
Zero Blunt TOPO Kit	ThermoFisher	451245
NEBuilder HiFi DNA Kit	New England Biolabs	E5520S
Illustra GenomiPhi V2 DNA Amplication Kit	GE Healthcare	GE 25-660-30
ULYSIS AF647 Nucleic Acid Labeling Kit	ThermoFisher	U21660
ULYSIS AF546 Nucleic Acid Labeling Kit	ThermoFisher	U21652
Centri-Sep Columns	Princeton Separation	CS-900
Qubit dsDNA HS assay kit	ThermoFisher	Q32851
QIAGEN Plasmid Midi Kit	QIAGEN	12143
Deposited Data		
Stowers Original Data Repository (ODR)	Stowers Institute for Medical Research	http://www.stowers.org/research/publications/odr
Stowers ImageJ Custom Plugins	Stowers Institute for Medical Research	research.stowers.org/imagejplugins/zipped_plugins.html
Experimental Model: Drosophila stocks used		
y w; +/+; +/+; sv$^{spa\text{-}pol}$	Hawley Lab	Wild Type (WT)
y w/Y^{+y}; Sp/SM1; sv$^{spa\text{-}pol}$	Hawley Lab	
FM7w; sv$^{spa\text{-}pol}$	Hawley Lab	
y w/Y^{+y}; Pr/TM3; sv$^{spa\text{-}pol}$	Hawley Lab	
FM7w/sc cv v f y^{+}; D/TM3	Hawley Lab	
y m{VASA-Cas9-3xGFP}ZH-2A-3xRFP w^{1118}/FM7c	Bloomington Stock Center	BLM 51323
y w; nosCas9	Bestgene	
y w; c(3)G$^{cc\Delta 1}$ca/TM3; sv$^{spa\text{-}pol}$	Hawley Lab	

y w/w^{+}; ru h th st cu c(3)G$^{cc\Delta 1}$ca/TM3; sv$^{spa-pol}$/+	Hawley Lab	
yw; ru h th st cu c(3)G $^{cc\Delta 1}$/TM3; pol	Hawley Lab	
yw; +/CyO; ru h th st cu c(3)G $^{cc\Delta 1}$ca/TM3	Hawley Lab	
y w; c(3)G $^{cc\Delta 2}$ca/TM3; sv$^{spa-pol}$		
yw; ru h th st cu c(3)G $^{cc\Delta 2}$/TM3; pol		
y w; c(3)G $^{cc\Delta 3}$ca/TM3; sv$^{spa-pol}$		
yw; ru h th st cu c(3)G $^{cc\Delta 3}$/TM3; pol		
net dpp dpy b pr cn	Hawley Lab	
ru h th st cu sr e ca	Hawley Lab	KAC81
attached-XY, y^{+} v f B; C(4)RM, ci ey^{R}	Hawley Lab	AD1
sc cv v f y^{+}/Bar[S]Y	Hawley Lab	U106
w^{1118}; In(2LR)Gla, wg^{Gla-1}/CyO; Herm{3xP3-ECFP,αtub-piggyBacK10}M10	BLM 32073	Transposase
Oligonucleotides		
tataCACCTGCattaCCGAcgctagtggctcctagagttcag	Ordered from IDT	Forward primer to PCR AarI C(3)G fragment *c(3)G $^{cc\Delta 1}$* (ckc102)
gcagCACCTGCgcggTTAAtgaaaaagaatttatagtcttaccattaggttatc	Ordered from IDT	Reverse primer to PCR AarI C(3)G fragment *c(3)G $^{cc\Delta 1}$* (ckc103)
gccgGCTCTTCNTAAcctttttctacaaaatgatttatt	Ordered from IDT	Forward primer to PCR SapI C(3)G fragment *c(3)G $^{cc\Delta 1}$* (ckc104)
gtatGCTCTTCNCGGtcatcaaaacatagtttagtatcg	Ordered from IDT	Reverse primer to PCR SapI C(3)G fragment *c(3)G $^{cc\Delta 1}$* (ckc105)
CTTCGAAAGCTTTGTTGGCCTCTAT	Ordered from IDT	Sense primer for gRNA plasmid *c(3)G $^{cc\Delta 1}$* (ckc113)
AAACATAGAGGCCAACAAAGCTTTC	Ordered from IDT	Antisense primer for gRNA plasmid *c(3)G $^{cc\Delta 1}$* (ckc114)
CTTCGCTCAATGCGATCTTCAAGCTGG	Ordered from IDT	Sense primer for gRNA plasmid *c(3)G $^{cc\Delta 2}$*
AAACCCAGCTTGAAGATCGCATTGAGC	Ordered from IDT	Anti-sense primer for gRNA plasmid *c(3)G $^{cc\Delta 2}$*
CTTCGATTGACTGATCAGGCAACGAGG	Ordered from IDT	Sense primer for gRNA plasmid *c(3)G $^{cc\Delta 2}$*

AAACCCTCGTTGCCTGATCAGTCAATC	Ordered from IDT	Anti-sense primer for gRNA plasmid *c(3)G* $^{cc\Delta 2}$
CTTCGCTCTTCCTGATTGCTGCGATGG	Ordered from IDT	Sense primer for gRNA plasmid *c(3)G* $^{cc\Delta 3}$
AAACTCGCAGCAATCAGGAAGAGC	Ordered from IDT	Anti-sense primer for gRNA plasmid *c(3)G* $^{cc\Delta 3}$
CTTCTCTTGAACAACAATCTGTCAAGG	Ordered from IDT	Sense primer for gRNA plasmid *c(3)G* $^{cc\Delta 3}$
AAACTGACAGATTGTTGTTCAAGAC	Ordered from IDT	Anti-sense primer for gRNA plasmid *c(3)G* $^{cc\Delta 3}$
gggttacactggctttcctt	Ordered from IDT	Genotyping primer for *c(3)G* $^{cc\Delta 3}$
ctgagactgtaattcctcgctaaa	Ordered from IDT	Genotyping primer for *c(3)G* $^{cc\Delta 3}$
accaacctcgtaggcatctg	Ordered from IDT	Genotyping primer for *c(3)G* $^{cc\Delta 2}$
GTTGAGAAGAAAAATTCAGAGCTCCG	Ordered from IDT	Genotyping primer for *c(3)G* $^{cc\Delta 2}$
Recombinant DNA		
pU6-BbsI-chiRNA-X204upstream	Vector backbone from Addgene	ID:45946
pHD-pBac-DsRed-X204HR	Vector backbone was a gift from Kate O'Conner-Giles Lab	
Software and Algorithms		
ImageJ	https://imagej.nih.gov/ij/	
Custom ImageJ plugins	research.stowers.org/imagejplugins/zipped_plugins.html	

1234